Monthly Notices
of the
ROYAL ASTRONOMICAL SOCIETY

Mon. Not. R. Astron. Soc. **419,** 1051–1069 (2012) doi:10.1111/j.1365-2966.2011.19762.x

The intriguing H I gas in NGC 5253: an infall of a diffuse, low-metallicity H I cloud?⋆

Á. R. López-Sánchez,[1,2,3]† B. S. Koribalski,[3] J. van Eymeren,[4] C. Esteban,[5,6] E. Kirby,[3,7] H. Jerjen[7] and N. Lonsdale[8]

[1]*Australian Astronomical Observatory, PO Box 296, Epping, NSW 1710, Australia*
[2]*Department of Physics and Astronomy, Macquarie University, NSW 2109, Australia*
[3]*CSIRO Astronomy and Space Science/Australia Telescope National Facility, PO Box 76, Epping, NSW 1710, Australia*
[4]*Universitaet Duisburg-Essen, Faculty of Physics, Lotharstr. 1, 47048 Duisburg, Germany*
[5]*Instituto de Astrofísica de Canarias, E-38200 La Laguna, Tenerife, Spain*
[6]*Departamento de Astrofísica, Universidad de La Laguna, E-38205 La Laguna, Tenerife, Spain*
[7]*Research School of Astronomy and Astrophysics, Australian National University, Cotter Rd. Weston, ACT 2611, Australia*
[8]*Centre for Astrophysics and Supercomputing, Swinburne University of Technology, PO Box 218, Hawthorn, Victoria 3122, Australia*

Accepted 2011 September 2. Received 2011 August 31; in original form 2011 March 18

ABSTRACT

We present new, deep H I line and 20-cm radio-continuum data of the very puzzling blue compact dwarf galaxy NGC 5253, obtained with the Australia Telescope Compact Array as part of the 'Local Volume H I Survey' (LVHIS). Our low-resolution H I maps show, for the first time, the disturbed H I morphology that NGC 5253 possesses, including tails, plumes and detached H I clouds. The high-resolution map reveals an H I plume at the SE and an H I structure at the NW that surrounds an Hα shell. This latter structure is related to an expanding bubble in the interstellar medium (ISM), but it will almost certainly not originate a galactic wind. We confirm that the kinematics of the neutral gas in NGC 5253 are highly perturbed and do not follow a rotation pattern. We discuss the outflow and infall scenarios to explain such disturbed kinematics, analyse the environment in which NGC 5253 resides and compare its properties with those observed in similar star-forming dwarf galaxies. The radio-continuum emission of NGC 5253 is resolved and associated with the intense star-forming region located at the centre of the galaxy. We complete the analysis using multiwavelength data extracted from the literature, which include X-ray, *Galaxy Evolution Explorer (GALEX)* far-ultraviolet, optical *B* and *R* band and Hα, near-infrared *H* band, and far-infrared data. We estimate the star formation rate using this multiwavelength approach, and compare the results with other galaxy properties. NGC 5253 does not satisfy the Schmidt–Kennicutt law of star formation, has a very low H I mass-to-light ratio when comparing with its stellar mass and seems to be slightly metal-deficient in comparison with starbursts of similar baryonic mass. Taking into account all available multiwavelength data, we conclude that NGC 5253 is probably experiencing the infall of a diffuse, low-metallicity H I cloud along the minor axis of the galaxy. The infall of this independent H I cloud is comprising the ISM and triggering the powerful starburst we see in NGC 5253. The tidally disturbed material observed at the east and north of the galaxy is a consequence of this interaction, which probably started more than 100 Myr ago. The origin of this H I cloud may be related with a strong interaction between NGC 5253 and the late-type spiral galaxy M83 in the past.

Key words: galaxies: abundances – galaxies: individual: NGC 5264 – galaxies: interactions – galaxies: ISM – galaxies: kinematics and dynamics – galaxies: starbursts.

⋆The observations were obtained with the Australia Telescope which is funded by the Commonwealth of Australia for operations as a National Facility managed by CSIRO.

†E-mail: alopez@aao.gov.au

1 INTRODUCTION

Multiwavelength analyses of local dwarf galaxies give the opportunity to study the impact of the star formation activity on both the interstellar medium (ISM) and the surrounding intergalactic medium (IGM), study the dynamics of galaxy evolution at both high and low spatial scales, and explore the triggering mechanisms of low-mass starbursting systems. In particular, nearby dwarf starbursts are excellent laboratories for investigating the properties of the star-forming regions, the behaviour and fate of the neutral, ionized and hot gas, and their effects on the stellar component of the galaxy, giving fundamental parameters to constrain models of the chemical and dynamical evolution of galaxies.

An intriguing local starburst galaxy is the blue compact dwarf galaxy (BCDG) NGC 5253 in the Centaurus A group (Karachentsev et al. 2007). The larger nearby galaxy to NGC 5253 is the late-type spiral M83, which is at a distance of 4.6 Mpc and lies at an angular distance of $1^\circ\,54'$ from NGC 5253. NGC 5253 is an ideal target for multiwavelength analyses of starburst galaxies, and a large amount of information is available at all frequencies. The outer optical isophotes of NGC 5253 resemble a dwarf elliptical galaxy, but Hα images (Martin 1998; Calzetti et al. 2004; Meurer et al. 2006) revealed its starbursting nature, as it shows a large amount of ionized gas. This includes a filamentary structure that is extending perpendicular to its optical major axis and reaches beyond the stellar distribution. The star formation activity is very intense in this galaxy. Indeed, NGC 5253 is considered as one of the youngest starbursts of the Universe (e.g. van den Bergh 1980; Moorwood & Glass 1982; Rieke, Lebofsky & Walker 1988; Caldwell & Phillips 1989) and even a large population of massive, young Wolf–Rayet (WR) stars has been reported in this galaxy (Campbell, Terlevich, & Melnick 1986; Kobulnicky et al. 1997; Schaerer et al. 1997; López-Sánchez et al. 2007; López-Sánchez & Esteban 2010a,b; Monreal-Ibero et al. 2010).

The winds of the WR stars seem to be polluting some internal areas of the galaxy centre, as a localized nitrogen enrichment (Walsh & Roy 1989; Kobulnicky et al. 1997; López-Sánchez et al. 2007; López-Sánchez & Esteban 2010a,b; Monreal-Ibero et al. 2010) and a possible slight helium enrichment (Campbell et al. 1986; López-Sánchez et al. 2007) have been reported. The highest oxygen abundance of the ionized gas found in NGC 5253 is $12+\log(\mathrm{O/H}) = 8.30$ (López-Sánchez et al. 2007), which corresponds to $\sim$40 per cent solar assuming $12+\log(\mathrm{O/H})_\odot = 8.66$ (Asplund, Grevesse & Sauval 2005). The very centre of the galaxy hosts an extremely luminous, compact, obscured (Alonso-Herrero et al. 2004) site of star formation, including some star clusters with ages younger than 10 Myr and masses between 10^5 and 10^6 $\mathrm{M}_\odot$ (e.g. Gonzalez-Riestra, Rego & Zamorano 1987; Calzetti et al. 1997; Harris et al. 2004; Vanzi & Sauvage 2004; Cresci, Vanzi & Sauvage 2005; Martín-Hernández, Schaerer & Sauvage 2005). Extended diffuse X-ray emission (Strickland & Stevens 1999; Summers et al. 2004) associated with the filamentary Hα structure is explained as superbubbles around the massive star-forming regions, and have been created by the combined action of supernova explosions and stellar winds. However, the radio spectral energy distribution of NGC 5253 is almost entirely dominated by thermal emission (Beck et al. 1996; Turner, Ho & Beck 1998), which implies the extreme youth of the starburst.

Despite all observational efforts, the behaviour of the neutral gas within NGC 5253 is far from clear. The first interferometric Very Large Array (VLA) observations (Kobulnicky & Skillman 1995), which only showed the H I map around the galaxy centre, revealed that the neutral gas either rotates about the minor axis of the galaxy or flows radially along the minor axis. NGC 5253 was observed with the radio-interferometer Australia Telescope Compact Array (ATCA) as part of the Local Volume H I Survey (LVHIS)[1] project (Koribalski 2008; Koribalski et al., in preparation). The preliminary LVHIS results (López-Sánchez et al. 2008) showed that the neutral gas is more extended than the optical size of the galaxy, revealing a peculiar morphology in its northern areas. These data also confirmed the intriguing kinematics of the H I emission. Later, Kobulnicky & Skillman (2008) (hereafter KS08) analysed high-resolution VLA data of the centre of NGC 5253 and found a redshifted H I plume extending to the SE along the minor axis and containing 20–30 per cent of the neutral gas. These authors speculated that this feature is either a dynamically distinct tidal remnant or an inflow on the far side of the galaxy. They also reported a starburst-blown bubble stalled by interaction with a massive neutral envelope at the NW of the galaxy. However, their data did not allow the analysis of the diffuse neutral gas in which NGC 5253 is embedded, which provides the key clues to understand all the peculiarities observed in this strong starbursting dwarf galaxy.

Here we present full synthesis of ATCA H I line data of the BCDG NGC 5253 to analyse its neutral gas distribution in both large and short scales. We also perform a comprehensive analysis of this peculiar system combining all available multiwavelength data. In addition, we use the ATCA H I data of the nearby dwarf galaxies ESO 444−G084, IC 4316 and NGC 5264 (Koribalski et al., in preparation) to compare the properties of NGC 5253 with those found in nearby dwarf galaxies within the Centaurus A group. This analysis will give clues to constrain the nature of the starburst phenomenon in NGC 5253. Table 1 compiles the basic properties of these four galaxies.

The paper is organized as follows. In Section 2 we summarize the observations and data reduction; Section 3 presents the ATCA H I line results (neutral gas distribution and kinematics) of our analysis of NGC 5253 and the comparison of the global H I spectrum with the H I Parkes All-Sky Survey (HIPASS) data. Section 4 compiles the 20-cm radio-continuum results. The discussion in Section 5 compares the H I morphology and kinematics [and other galaxy properties, as the star formation rate (SFR), stellar mass, chemical abundances and mass-to-light ratios] of NGC 5253 with those found in similar starbursts reported in the literature and in the nearby dwarf galaxies, as well as analyses the environment in which NGC 5253 resides. Section 6 contains our conclusions.

2 OBSERVATIONS AND DATA REDUCTION

H I line and 20-cm radio-continuum observations of the galaxies NGC 5253, ESO 444−G084, IC 4316 and NGC 5264 were obtained simultaneously with the ATCA. This radio-interferometer consists of six 22-m antennae, hence giving 15 baselines in a single configuration. Our data were obtained between 2005 January and 2009 January using three or four different array configurations. For NGC 5253, we used the EW367, 750A, 1.5A and 6A array configurations (the observational details of the other galaxies can be found in Koribalski et al. 2011). Each galaxy was observed for a full synthesis ($\sim$12 h) in each array to ensure an excellent *uv*-coverage and sensitivity to detect structures on all scales. Whereas the short baselines recover the extended H I distribution, the larger baselines provide the details needed to compare with UV/optical/IR data (e.g.

[1] http://www.atnf.csiro.au/research/LVHIS

Table 1. Basic properties of the BCDG NGC 5253 and the dwarf irregular galaxies ESO 444−G084, IC 4316 and NGC 5264.

Name	NGC 5253	IC 4316	ESO 444−G084	NGC 5264	Ref.
HIPASS	J1339−31A	J1340−28	J1337−28	J1341−29	
Centre position	$13^h\,39^m\,55\overset{s}{.}9$	$13^h\,40^m\,18\overset{s}{.}4$	$13^h\,37^m\,20\overset{s}{.}0$	$13^h\,41^m\,36\overset{s}{.}7$	(1), (2), (3), (4)
α, δ(J2000)	$-31^\circ\,38'\,24''$	$-28^\circ\,53'\,32''$	$-28^\circ\,02'\,42''$	$-29^\circ\,54'\,47''$	
l, b	$314\overset{\circ}{.}86$, $30\overset{\circ}{.}11$	$315\overset{\circ}{.}66$, $30\overset{\circ}{.}77$	$315\overset{\circ}{.}12$, $33\overset{\circ}{.}74$	$315\overset{\circ}{.}72$, $31\overset{\circ}{.}71$	(1), (2), (3), (4)
$v_{\rm opt}$ (km s^{-1})	381 ± 3	674 ± 43	587 ± 3	478 ± 3	(5), (6), (6), (7)
Type	Im pec, H II, Sbrst	IBm? pec	Im	IB(s)m	(6), (6), (6), (6)
Distance (Mpc)[a]	$4.0^{+0.2}_{-0.4}$	4.41	4.60	4.50	(8), (9), (9), (9)
1 arcsec (pc)	19.4	21.4	22.3	21.8	
Optical diametre	5.0×1.9 arcmin^2	1.7×1.1 arcmin^2	1.3×1.0 arcmin^2	2.5×1.5 arcmin^2	(6), (7), (6), (7)
Optical diametre	5.8×2.2 kpc^2	2.2×1.4 kpc^2	1.74×1.4 kpc^2	3.3×2.0 kpc^2	
A_B (mag)[b]	0.242, 0.70	0.237	0.295	0.223	(10,11), (10), (10), (10)
m_B (mag)	10.09 ± 0.01	14.73 ± 0.21	14.71 ± 0.09	12.36 ± 0.09	(11), (6), (7), (7)
m_H (mag)	8.48±0.02	13.9 ± 0.2	...	10.85 ± 0.07	(11), (TW), (...), (4)
$B-H$	1.61 ± 0.04	0.83 ± 0.41	...	1.51 ± 0.16	(11), (TW), (...), (TW)
M_B (mag)	-17.92 ± 0.01	-13.49 ± 0.21	-13.60 ± 0.09	-15.91 ± 0.09	(12), (TW), (TW), (TW)
L_B (10^8 L$_\odot$)[c]	22.9 ± 0.2	0.39 ± 0.07	0.43 ± 0.04	3.50 ± 0.26	(12), (TW), (TW), (TW)
$M_{\rm star}$ (10^8 M$_\odot$)[d]	11.4 ± 0.5	0.094 ± 0.024	0.12[e]	1.63 ± 0.13	(12), (TW), (TW), (TW)
12+log(O/H)	8.18 (A), 8.28 (C) ± 0.04	8.16 ± 0.20	7.37 ± 0.20	8.50 ± 0.20	(5), (13), (14,TW), (14,TW)

[a]The errors quoted in NGC 5253 have been estimated by taking into account all available measurements (see Section 5.2). For the rest of the galaxies, the distance has been obtained from Karachentsev et al. (2002), who did not quote any uncertainties in their measurements.
[b]Except for NGC 5253, the A_B value tabulated here corresponds to the Galactic extinction (Schlegel, Finkbeiner & Davis 1998). All magnitudes and colours compiled in this table have been corrected for extinction using the A_B value and following the prescriptions given by López-Sánchez & Esteban (2008).
[c]The B-band luminosity, L_B, is calculated from the extinction-corrected B-band absolute magnitude, using a solar B-band magnitude of 5.48 mag (Bessel, Castelli & Plez 1998).
[d]The total stellar mass, $M_{\rm star}$, was computed from the extinction-corrected H-band absolute magnitude, assuming an H-band mass-to-light ratio of $M_{\rm star}/L_H = 0.8$. The H-band luminosity, L_H, is calculated from the H-band absolute magnitude, using a solar H-band magnitude of 3.35 mag (Colina, Bohlin & Castelli 1996). See Kirby et al. (2008) and López-Sánchez (2010) for details.
[e]For ESO 444−G084 we computed a tentative value of $M_{\rm star}$ assuming $B-H = 1.0$ mag.
References: (1) Turner & Beck (2004); (2) Jones et al. (2005); (3) Kaldare et al. (2003); (4) Skrutskie et al. (2006); (5) López-Sánchez et al. (2007); (6) de Vaucouleurs et al. (1991); (7) Lauberts & Valentijn (1989); (8) Karachentsev et al. (2004); (9) Karachentsev et al. (2002); (10) Schlegel et al. (1998) ; (11) López-Sánchez & Esteban (2008); (12) López-Sánchez (2010); (13) Lee, Zucker & Grebel (2007); (14) Lee, Grebel & Hodge (2003); and (TW) this value has been computed in this work.

Koribalski & López-Sánchez 2009). The data in the three most compact array configurations are part of the LVHIS project (Koribalski et al. 2011), while the data in the most extended ATCA configuration are provided by our multiwavelength analysis of a sample of nearby BCDGs (López-Sánchez et al. 2009a,b; López-Sánchez et al., in preparation).

Two different frequency bands are always available at the ATCA. We used the first frequency band (IF1) to get the 21-cm line data of neutral hydrogen (which has a rest frequency of 1420.406 MHz) and the second frequency band (IF2) to get the 20-cm radio-continuum data. IF1 was centred on 1418 MHz with a bandwidth of 8 MHz, divided into 512 channels. This gives a channel width of 3.3 km s^{-1} and a velocity resolution of 4 km s^{-1}. The ATCA primary beam is 33.6 arcmin at 1418 MHz. IF2 was centred on 1384 MHz (20 cm) with a bandwidth of 128 MHz divided into 32 channels.

Flux calibration was performed by observations of the primary ATCA calibrator, PKS 1934−638, which has a flux of 14.95 Jy at 1418 MHz. The phase calibration was achieved by periodic observations (every 30 min) of the bright calibration source PKS 1308−220, which has a flux of 5.04 Jy at 1418 MHz. Data reduction was carried out with the MULTICHANNEL IMAGE RECONSTRUCTION, IMAGE ANALYSIS AND DISPLAY (MIRIAD) software package (Sault, Teuben & Wright 1995) using standard procedures. After calibration, the IF1 data were split into a narrow-band 20-cm radio-continuum and an H I line data set using a first-order fit to the line-free channels.

By combining data from several array configurations we achieve a very good *uv*-coverage and, hence, the Fourier transformation of the obtained visibilities allows us to make data cubes and images at a large range of angular resolutions. This is achieved by choosing different weightings for short, medium and long baselines, which in turn are sensitive to different structure scales. The weighting of the data does not only affect the resolution, but also the rms noise and sensitivity to diffuse emission. For our analysis, H I cubes were made using 'natural' (na) and 'robust' ($r = 0$) weighting of the *uv*-data in the velocity range covered by the H I emission using steps of 4 km s^{-1}. The longest baselines to the distant antenna six (CA06) were excluded when making the low-resolution ('na' weighting) and the intermediate-resolution cubes ($r = 0$ weighting), but they were considered to get the high-resolution cube. Broad-band 20-cm radio-continuum images were made using 'robust' ($r = 0$) weighting of the IF2 *uv*-data and excluding the baselines to CA06. The moment maps (integrated intensity map, intensity-weighted mean velocity field and the velocity dispersion) were created from the H I data cubes by first isolating the regions of significant emission in every channel and afterwards clipping everything below a $\sim 2\sigma$ threshold.

3 H I RESULTS

3.1 The H I distribution of NGC 5253

The distribution of atomic neutral gas within the BCDG NGC 5253 is shown in Fig. 1. This multiwavelength colour image compares our new low-resolution H I map (in dark blue) with the ionized

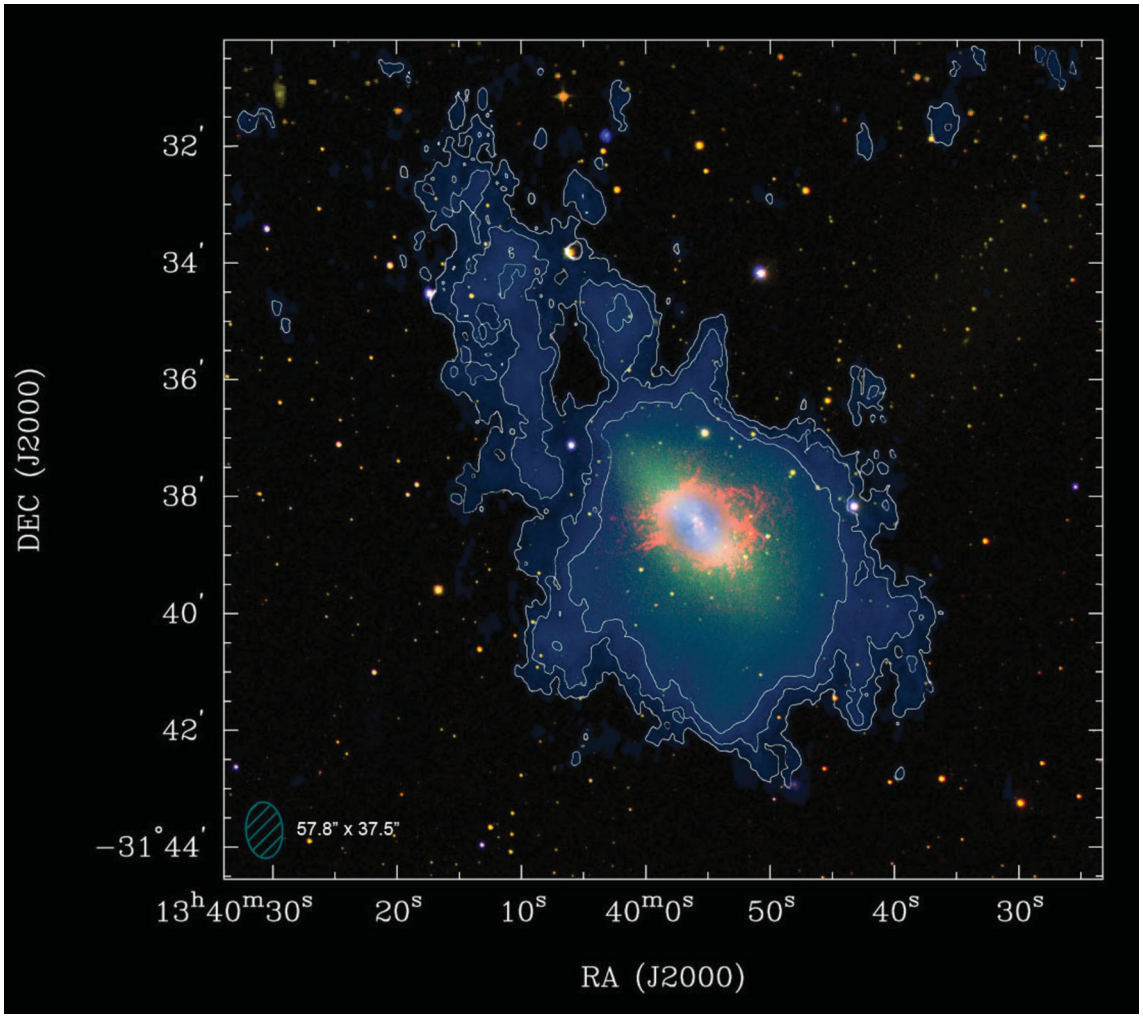

Figure 1. Colour image of the BCDG NGC 5253 obtained combining data in *FUV* and *NUV* (cyan, *GALEX*), *R* band (green; Meurer et al. 2006) and Hα (red; Meurer et al. 2006), NIR *J* band [(orange, The Two Micron All Sky Survey (Skrutskie et al.) (2MASS)], and our ATCA low-resolution H I map (dark blue). The synthesized beam of the H I map is 57.8 × 37.5 arcsec^2. The plotted contour levels are 0.10 ($\sim 3\sigma$), 0.18 and 0.3 Jy beam^{-1} km s^{-1}.

gas emission (red) and the stellar component (in green). As we see, our new H I map, which is deeper than the previous VLA maps obtained by Kobulnicky & Skillman (1995) and KS08, clearly shows the diffuse atomic gas emission in the external regions of NGC 5253. Indeed, our low-resolution H I map, which is tracing the large-scale structures of the neutral gas component of the galaxy, clearly indicates that the atomic hydrogen gas is more extended than the optical size of the galaxy ($\sim 11 \times 6$ arcmin^2 = 12.8 kpc × 7 kpc, i.e. $\sim 2.2 \times 3.2$ times its optical size), showing a very peculiar morphology in its northern area. This region shows a kind of filamentary and disturbed H I morphology, which may suggest the existence of tidally disturbed material surrounding the galaxy. The southern region of NGC 5253 also shows a somewhat disturbed morphology, but in this case the H I gas is not as disrupted as it is seen at the northern regions.

Fig. 2 shows the low- and intermediate-resolution H I moment maps of NGC 5253. The H I distribution in these maps is shown up to 0.10 and 0.04 Jy beam^{-1} km s^{-1} ($\sim 3\sigma$ over the noise level), which corresponds to an H I column density of 5.1×10^{19} and 6.0×10^{19} atoms cm^{-2} for the low- and intermediate-resolutions maps, respectively. The H I maximum coincides with the optical centre of the galaxy, although the peak of the H I distribution seems to be displaced to the SE with respect to the optical component of the galaxy.

The H I emission in our low-resolution data cube covers a velocity range of 330 to 480 km s^{-1}. Assuming that the distance to NGC 5253 is 4.0 Mpc (see Table 1) and an integrated flux density of 42.1 ± 2.3 Jy km s^{-1}, we derive a total H I mass of $(1.59 \pm 0.09) \times 10^8$ M$_\odot$. The integrated flux in the northern disturbed areas is ∼5 per cent of the total flux of the galaxy, which corresponds to a mass of $\sim 8 \times 10^6$ M$_\odot$.

The intermediate-resolution map recovers 81 per cent of the total flux we detect in our low-resolution map, which mainly corresponds to the emission from the main body of the galaxy. Indeed, the intermediate-resolution map does not show the diffuse emission at the northern areas, although some disturbed material at the south-east can still be observed. This region corresponds to the feature that KS08 designed as the 'SE H I plume'. We note that this structure is more extended than that reported by these authors, as it extends ∼3.5 arcmin from the centre of the galaxy (the low-resolution map presented by KS08 only shows ∼1.5 arcmin). Hence, at this resolution the H I distribution in NGC 5253 does not follow its optical major axis but the neutral gas is rather distributed along the minor axis. Furthermore, this distribution is not symmetrical, as the SE region

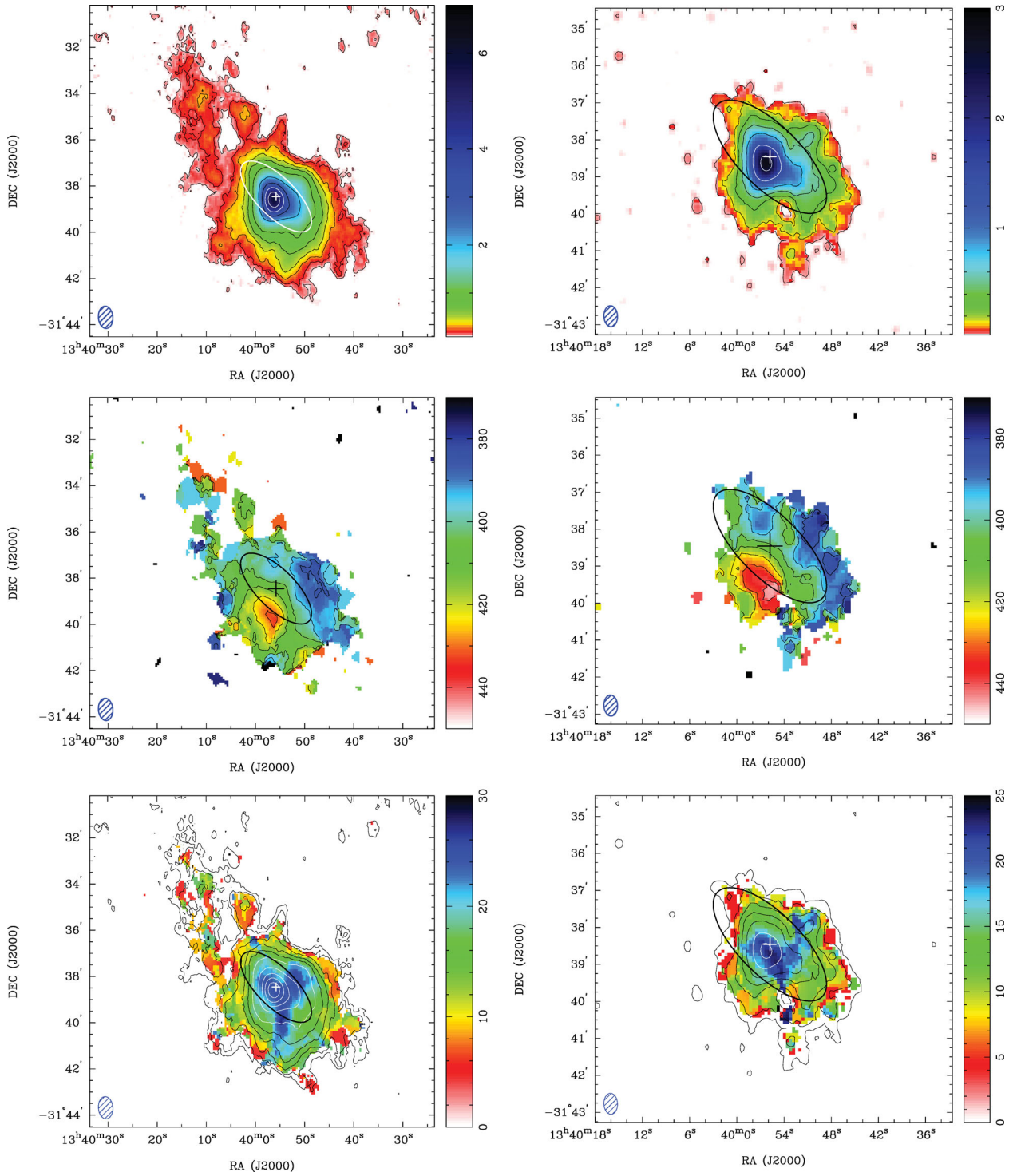

Figure 2. H I moment maps of the galaxy NGC 5253 as obtained from the ATCA, excluding baselines to CA06 and using 'natural' weighting (low-resolution data cube; left-hand column) and 'robust' ($r = 0$) weighting (intermediate-resolution data cube; right-hand column). The synthesized beam (57.8 × 37.5 arcsec^2 and 33.9 × 22.1 arcsec^2 for the low- and intermediate-resolution data cube, respectively) is displayed in the bottom-left corner of each panel. Note that the scale is different for the right- and left-hand maps. The galaxy centre is always marked with a cross, while an ellipse indicates the size of the optical appearance of the galaxy. Top row: H I distribution (moment 0 map) of NGC 5253; the scale is logarithmic. Contour levels are: 0.10 ($\sim 3\sigma$), 0.18, 0.3, 0.45, 0.65, 1, 2, 3, 4 and 5 Jy beam^{-1} km s^{-1} (low-resolution data cube) and 0.04 ($\sim 3\sigma$), 0.15, 0.3, 0.8, 1.5 and 2.5 Jy beam^{-1} km s^{-1} (intermediate-resolution data cube). Middle row: intensity-weighted mean, masked H I velocity field (moment 1 map); the contour levels range from 360 to 460 km s^{-1}, in steps of 4 km s^{-1}. Bottom row: H I velocity dispersion (moment 2 map), the range is from 0 to 30 km s^{-1} (low-resolution data cube) and to 25 km s^{-1} (intermediate-resolution data cube). We overlay the same moment 0 contours we used in the top row maps.

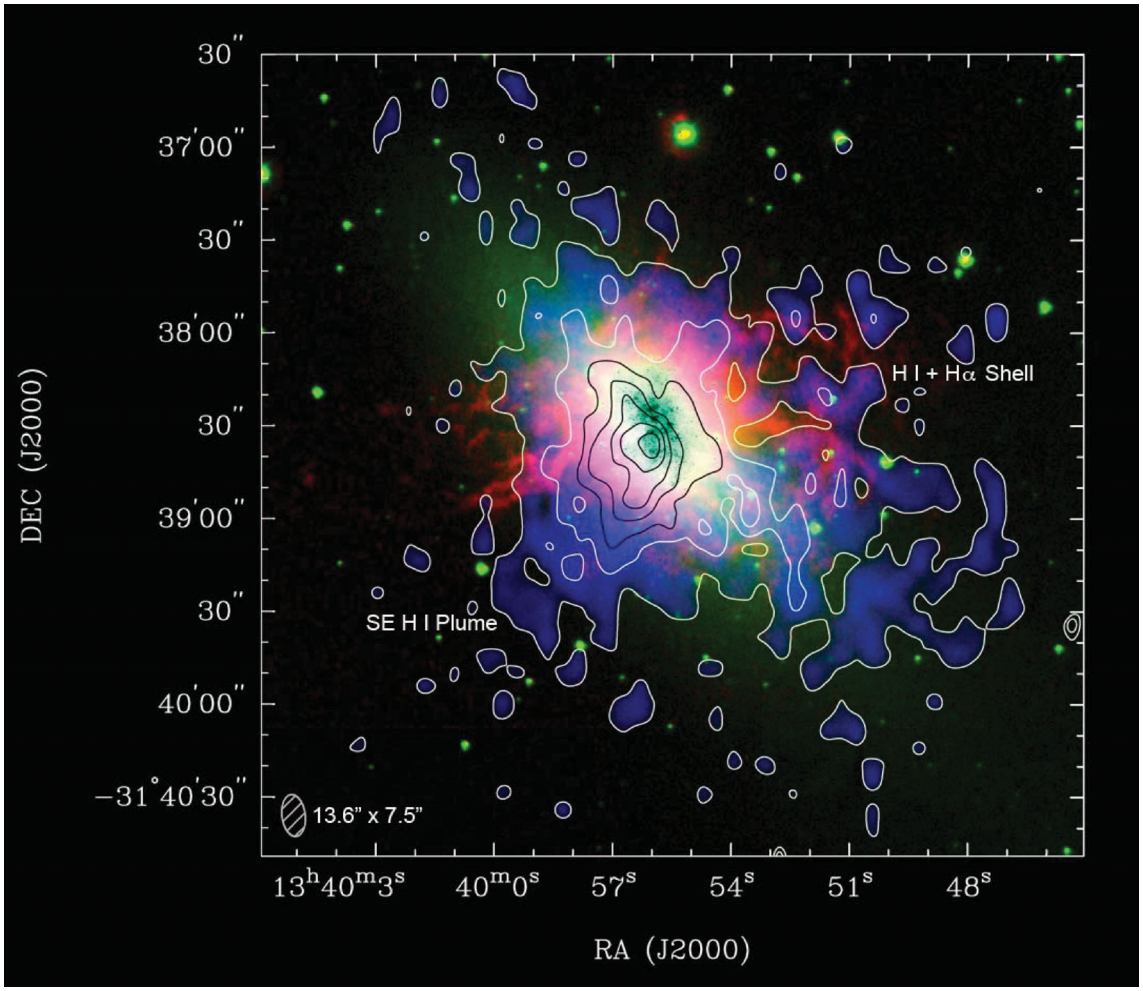

Figure 3. Contours of the high-resolution H I map (using 'robust', $r = 0$, weighting and including baselines to CA06) overlaid on to a colour image which combines *R* band and *FUV* band (green), Hα (red) and the ATCA high-resolution H I map (blue). The synthesized beam (13.6×7.5 arcsec^2) is displayed at the bottom-left corner. The contour levels are 0.032 (3σ), 0.12, 0.22, 0.32, 0.42, 0.52 and 0.62 Jy beam^{-1} km s^{-1}. Note the H I shell surrounding the NW Hα shell and the H I plume (without any Hα emission associated with it) at the SE, as they were previously noticed by KS08 using VLA data (see their fig. 3).

corresponds to the H I plume. Our intermediate-resolution H I maps also suggest that this feature is not just a plume but appears to be an open-shell structure. Most remarkably, the intermediate-resolution H I maps show a hole in the neutral gas emission just at the south of the galaxy and at the west of the 'SE H I plume'. This H I hole does not correspond to any of the bubbles that are surrounded by the ionized gas.

The high-resolution H I map of NGC 5253 is shown in Fig. 3, which displays the H I contours overlaid on to a multiwavelength colour picture which combines the Hα image of the galaxy (red) obtained by Meurer et al. (2006), the *R* band and *Galaxy Evolution Explorer* (*GALEX*) *FUV*-band images (green) and our high-resolution H I map (blue). The synthesized beam of our high-resolution H I map is 13.6×7.5 arcsec^2. The lowest contour level plotted in Fig. 3 corresponds to 0.032 Jy beam^{-1} km s^{-1} ($\sim 3\sigma$ over the noise level), which corresponds to an H I column density of 3.5×10^{20} atoms cm^{-2} assuming that the gas fills the beam. Our high-resolution H I map traces the highest density H I gas (which corresponds to the small-scale structures) and agrees quite well with the H I map presented by KS08. Indeed, both maps have quite a similar resolution (their synthesized beam is 9.0×7.6 arcsec^2) and sensitivity (assuming that the gas fills the beam, the lowest H I contour of the high-resolution H I map shown by KS08 corresponds to an H I column density of 6.0×10^{20} atoms cm^{-2}). Our map clearly recovers the three main H I features reported by these authors:

(1) the extensions following the optical major axis (in the direction NE–SW and that we clearly identify in the low- and intermediate-resolution maps),

(2) the 'SE H I plume' (that extends beyond the optical component of the galaxy, as it is seen in Fig. 3),

(3) the open shells at the west and east.

In particular, Fig. 3 shows an excellent correspondence between an Hα shell located at the NE and the H I gas in this region. Indeed, the H I peak column densities coincide with the Hα peaks in this area. Furthermore, both the neutral and ionized gas have a hole in the centre of this region, which also shows high values in its H I velocity dispersion (moment 2 maps in Fig. 2). We derive a neutral hydrogen mass of $\sim 5.4 \times 10^6$ M$_\odot$ in this H I shell, which matches the mass estimation given by KS08.

On the other hand, we do not see any correspondence between the neutral and the ionized gas in the Hα shell located at the east of the galaxy (see Fig. 3). The only appreciable H I feature in this zone is the 'SE H I plume', which lies just at the south of the Hα shell

located at the east of the galaxy, but this H I plume does not embed any Hα emission.

We also note that Fig. 3 shows some residual H I emission following the major axis of the galaxy, especially towards the SW, which was not detected in the maps shown by KS08.

3.2 Integrated galaxy spectra and comparison with HIPASS

Table 2 compiles the ACTA H I measurements and their derived properties. Interferometric data usually underestimate the total flux because of the missing short baselines, which filters out any extended diffuse H I emission. Hence, we compare the integrated spectrum obtained for each galaxy with the single-dish spectrum provided by the HIPASS (Barnes et al. 2001; Koribalski et al. 2004).

The HIPASS spectrum of each galaxy was extracted from the raw HIPASS data cubes assuming a point source (their intrinsic size is smaller than the ∼16 arcmin angular resolution of the gridded data) within a region of 20 × 20 arcmin^2 centred on the source, with each pixel weighted according to the expected beam response. Following the procedure described in Koribalski et al. (2004) and revisited by Kirby et al. (2011), we derived the basic spectral properties of the galaxies, which for NGC 5253, ESO 444−G084 and NGC 5264 are virtually identical to those compiled in the HIPASS Bright Galaxy Catalogue (Koribalski et al. 2004). Similar single-dish values for integrated H I properties of these three galaxies are provided by the HIDEEP Survey (Minchin et al. 2003). Table 2 also compiles our single-dish H I results.

Fig. 4 shows a comparison between the global H I line spectrum as obtained from HIPASS (dashed blue line) and LVHIS (solid black line) for NGC 5253. The agreement is quite good; LVHIS data recover almost 96 per cent of the single-dish H Iflux, suggesting that very little diffuse H I emission has been filtered out in our interferometric observations.

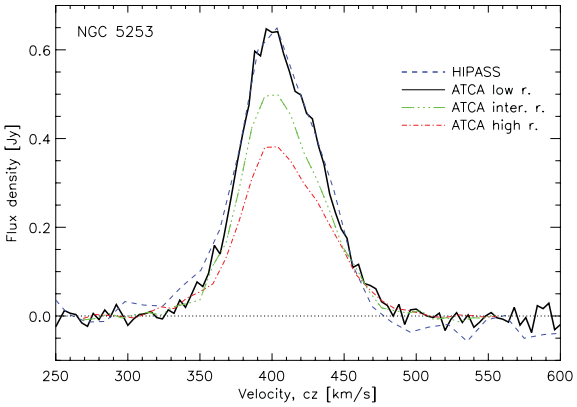

Figure 4. The global H I line spectrum of NGC 5253 as obtained from HIPASS (dashed blue line) and LVHIS using the low-resolution data cube (solid black line). The zero baseline is plotted with a dotted black line. We also include the global H I line spectra derived using the intermediate-resolution (dash–dotted red line) and the high-resolution (dash–dotted green line) data cubes.

3.3 The H I kinematics of NGC 5253

The central panels in Fig. 2 show the mean, masked low- and intermediate-resolution H I velocity field of the galaxy. As previously noticed by Kobulnicky & Skillman (1995), the most remarkable characteristic of these maps is that the neutral gas *is not* rotating about the optical minor axis of the galaxy (as it should be expected) but *it seems to rotate about its optical major axis*, as it happens in polar ring galaxies, or it just flows radially along the minor axis. Later, KS08 used high-resolution maps to discard the rotation scenario, emphasizing that their new data are more consistent with either an inflow or outflow of neutral gas along the minor axis from the south and east of the nucleus.

Table 2. ATCA H I measurements and derived properties. We also list the main properties derived from available single-dish (Parkes) observations, which were compiled in the HIPASS Bright Galaxy Catalogue (Koribalski et al. 2004) for NGC 5253, ESO 444−G084 and NGC 5264 and in Minchin et al. (2003) for IC 4316.

Name	NGC 5253	IC 4316	ESO 444−G084	NGC 5264
HIPASS	J1339−31A	J1340−28	J1337−28	J1341−29
ATCA properties				
H I diameter (arcmin × arcmin^2)	11 × 7	4 × 3	3 × 5	5.5 × 6.5
H I/opt. diameter ratio	∼2.2 × 3.2	∼2.4 × 2.7	∼2.3 × 5.0	∼2.2 × 4.3
Velocity range (km s^{-1})	334–480	550–610	530–640	440–510
$v_{\rm sys}$ (km s^{-1})	404 ± 1	579 ± 2	586 ± 1	477 ± 1
w_{50} (km s^{-1})	63 ± 2	22 ± 4	52 ± 2	30 ± 2
w_{20} (km s^{-1})	95 ± 3	40 ± 6	72 ± 3	43 ± 3
H I flux density ($F_{\rm HI}$) (Jy km s^{-1})	42.1 ± 2.3	2.68 ± 0.24	19.9 ± 1.3	8.78 ± 0.73
H I mass ($M_{\rm HI}$) (10^8 M$_\odot$)	1.59 ± 0.09	0.123 ± 0.011	0.992 ± 0.065	0.419 ± 0.036
$M_{\rm HI}/L_B$ (M$_\odot$/L$_\odot$)[a]	0.069 ± 0.004	0.313 ± 0.034	2.29 ± 0.18	0.116 ± 0.009
$M_{\rm gas}/M_{\rm stars}$ (per cent)[b]	18.4 ± 1.3	173 ± 46	∼1091	33.9 ± 4.0
Single-dish properties				
H I flux density ($F_{\rm HI}$) (Jy km s^{-1})	44.0 ± 4.5	2.1 ± 0.2	18.5 ± 2.7	12.3 ± 1.9
H I mass ($M_{\rm HI}$) (10^8 M$_\odot$)	1.66 ± 0.16	0.096 ± 0.009	0.922 ± 0.013	0.59 ± 0.09
$M_{\rm HI}/L_B$ (M$_\odot$/ L$_\odot$)[a]	0.072 ± 0.007	0.25 ± 0.03	2.12 ± 0.32	0.162 ± 0.026
$M_{\rm gas}/M_{\rm stars}$ (per cent)[b]	19.2	135	1014	48
$M_{\rm bar}$ (10^8 M$_\odot$)[c]	13.6 ± 0.7	0.221 ± 0.036	1.34	2.41 ± 0.25

[a]The H I-mass-to-light ratio, $M_{\rm HI}/L_B$, is a distance-independent quantity that was computed following $M_{\rm HI}/L_B = 1.5 \times 10^{-7} F_{\rm HI} \times 10^{0.4 m_B}$, with $m_B = m_B^{NC} - A_B$ (Warren, Jerjen & Koribalski 2004).
[b]The total mass of the neutral gas, $M_{\rm gas}$, was computed assuming $M_{\rm gas} = 1.32 \times M_{\rm HI}$.
[c]The baryonic mass, $M_{\rm bar}$, was computed assuming $M_{\rm bar} = M_{\rm stars} + M_{\rm gas}$.

Here we will consider both scenarios to try to explain the intriguing and disturbed H I kinematics of NGC 5253.

Figs 5–7 show, respectively, the low-, intermediate- and high-resolution H I channel maps of NGC 5253. As we see, the H I distribution is asymmetric and does not show any clear rotational pattern. To facilitate the analysis of the H I kinematics within this peculiar BCDG, we plot in Figs 9 and 10 some position–velocity (PV) diagrams across our H I data cubes. The position angle (PA) and localization of these slits are shown in Fig. 8. The results found in our analysis are the following.

(1) The PV diagram along the optical major axis of NGC 5253 (with a PA of 45°) is plotted in the top panel of Fig. 9. The neutral gas seems to show a constant velocity along the slit, with a velocity almost coincident with the systemic velocity ($\sim$410 km s^{-1}). However, the central regions show an elongation to higher velocities ($\sim$470 km s^{-1}). A not so obvious elongation to lower velocities ($\sim$350 km s^{-1}) is also observed in the same region. Indeed, the channel maps almost always show H I emission in the centre of the galaxy. However, the velocity minimum is located at $\sim$1.25 arcmin from the position of the velocity maximum. This feature seems to be a reminiscent of a rotation pattern which follows the optical major axis of the galaxy. KS08 already suggested the presence of such a feature in their high-resolution H I maps (see their fig. 9), but our PV diagram (which shows H I emission $\sim$10 arcmin along the optical major axis) shows this behaviour more clearly. We also note that there are two maxima in the H I emission just in the very centre of the galaxy, which may suggest the existence of two main entities, as we will discuss below.

(2) The PV diagram along the optical minor axis of NGC 5253 (with a PA of 135°, which is plotted in the bottom panel of Fig. 9) shows an evident velocity gradient of the neutral gas, from $\sim$470 km s^{-1} at the east to $\sim$350 km s^{-1} at the west. That is the main velocity field that we obtain in the first moment maps (see Fig. 2). We also detect two H I peaks in this PV diagram embedded in two structures that have different orientations. From the western peak towards the west, the velocity decreases continuously from $\sim$400 to $\sim$350 km s^{-1}. However, the eastern region (which corresponds to the 'SE H I plume') shows a decrease in the velocity from the eastern H I peak ($\sim$440 km s^{-1}) to the east ($\sim$400 km s^{-1}). The observed overall sinusoidal pattern, which is the characteristic of interactions between two objects, is also found in the intermediate- and high-resolution data cubes.

(3) The intermediate-resolution H I channel maps of NGC 5253 show two open bubbles or shells at the NW (between 359 and 386 km s^{-1}) and at the SE (between 404 and 422 km s^{-1}). These features may correspond to outflows of material originated in the central starburst. We individually analyse these two features.

(a) The NW shell corresponds to a bubble of neutral and ionized gas ('H I+Hα Shell' in Fig. 3) that is originated in the densest regions of the ISM. Indeed, this structure, which has a size of $\sim$0.8–1 kpc, is traced by fragmented H I gas in the 377–413 km s^{-1} channel maps of the high-resolution H I data cube (Fig. 7). The 'NW H I+Hα shell' was already detected by KS08, who noticed that the H I velocity range (30–40 km s^{-1}) is comparable to that found in the ionized gas. The non-detection of the X-ray emission indicates that it has not been produced by the most recent star formation event, but it originated $\sim$40 Myr ago.

(b) The 'SE H I shell' (between 404 and 422 km s^{-1} in Fig. 6) has lower H I column densities than those seen in the NW shell. The eastern areas actually correspond to the 'SE H I plume' reported by KS08 and has no counterpart to any Hα or X-ray emission. This shell has a very large size, $\sim$1.8–2 kpc, i.e. it is twice as large as the 'NW H I+Hα shell', and as large as the optical minor axis of the galaxy. We do not consider that this structure has originated by an outflow. A careful analysis of the previous (368–395 km s^{-1}) and later (431–449 km s^{-1}) channel maps indicates a continuous evolution of the H I gas from the NW to the SE (along the optical minor axis, the SE region corresponds to the 'SE H I plume') and from the NE to the SW (along the optical major axis), which may correspond to two different entities.

(4) The disturbed northern region observed in the low-resolution H I distribution map is composed of several small H I clouds, which have a relatively large range of velocities (386 to 458 km s^{-1}). We identify two main structures which do not show any stellar counterpart and are not related to any Hα emission, suggesting that both have a tidal origin.

(a) The brightest of the H I clouds is located just at the north of the NE end of the stellar distribution of the galaxy. This 'N H I cloud' has a total H I mass of $\sim$2.0 $\times$ 10^6 M$_\odot$ and it is connected to the main body of the galaxy by diffuse neutral gas.

(b) The elongated and narrow H I tail at the NE of the system consists of a chain of several H I clumps. Although they have a relatively constant velocity of around 400 km s^{-1}, the clumps also show some variations in velocity following a kind of sinusoidal pattern with an amplitude of $\sim$20–30 km s^{-1} (see the top panel of Fig. 10). The total H I mass in the 'NE H I tail' is $\sim$4.2 $\times$ 10^6 M$_\odot$. It is very interesting to note that there is a smooth transition in both position and velocity between the eastern tip of the SE H I plume (which has a velocity of $\sim$400 km s^{-1}) and the 'NE H I tail' (which has a similar radial velocity in this area).

(5) Finally, some channel maps show long plumes of neutral gas extending from the H I maxima towards the external regions of the galaxy. Especially evident are the features seen in the 368–386 km s^{-1} and in the 431–440 km s^{-1} channel maps (the later structure corresponds to the 'SE H I plume'), which are both spatially coincident at the southern regions of NGC 5253. Indeed, the PV diagram crossing this region (bottom panel of Fig. 10) clearly shows two independent H I peaks embedded in a sinusoidal pattern. The 'SE H I plume' increases velocity from the east ($\sim$400 km s^{-1}) to the centre of NGC 5253 ($\sim$460 km s^{-1}), but then this tendency is broken, as the velocity of the SW region decreases from the centre of the galaxy ($\sim$410 km s^{-1}) to the external western areas ($\sim$350 km s^{-1}). We notice that if we consider both structures as a single entity the global kinematical pattern is a decrease in the velocities from the east ($\sim$460 km s^{-1}) to the west ($\sim$350 km s^{-1}), which could be incorrectly attributed to rotation. As we discussed before, the 'SE H I plume' is not associated with any of the structures observed in the Hα images, and hence its outflow origin can be discarded (see also KS08). Therefore, the most plausible explanation of the sinusoidal pattern is that we are observing two different entities that are now in interaction. The 3D analysis of the low- and intermediate-resolution data cubes indicates a continuity between the features located at the NW regions (as the western H I peak in the 368 km s^{-1} channel map) with the 'SE H I plume' following the minor axis, which continues to the diffuse tidal material at the NE. This complete entity seems to be an independent system which is falling into NGC 5253. The main body of the galaxy would then correspond to the SW and NE areas, which are aligned with the optical major axis and is still rotating.

In summary, these new, deep H I data seem to indicate that the neutral gas found in the northern areas of the galaxy has a tidal

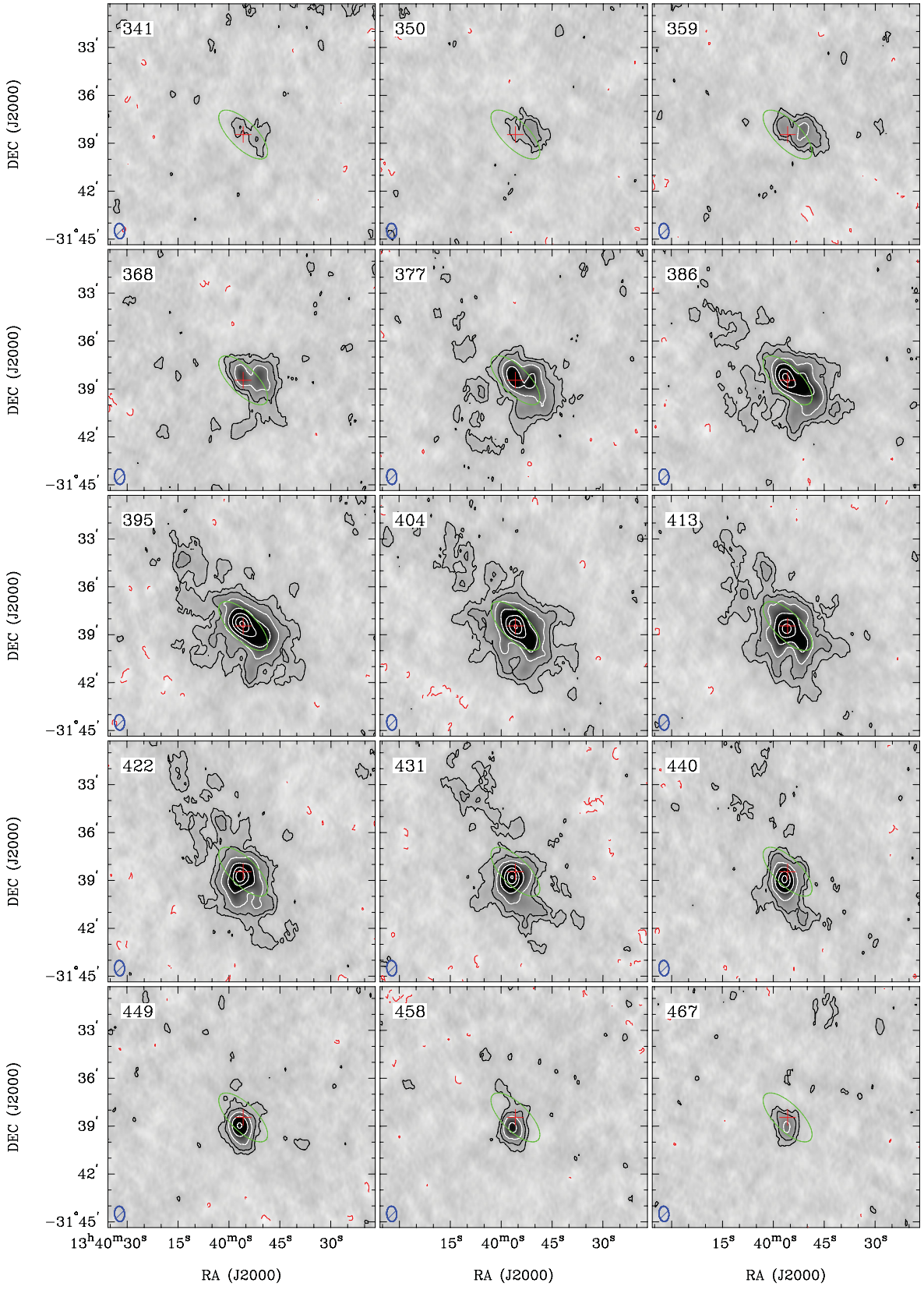

Figure 5. H I channel maps, in steps of 9 km s^{-1}, of the BCDG NGC 5253 as obtained from the ATCA, using 'natural' weighting and excluding baselines to CA06 (low-resolution data cube). The contour levels are −3 (dashed red contours), 3 (∼2.8σ), 6, 12, 24, 45, 65 and 85 mJy beam^{-1}. The galaxy centre is marked with a red cross, while the green ellipse corresponds in size to the optical appearance of the galaxy. The centre velocity of each channel is displayed at the top-left and the synthesized beam (57.8 × 37.5 arcsec^2) at the bottom-left corner of each panel.

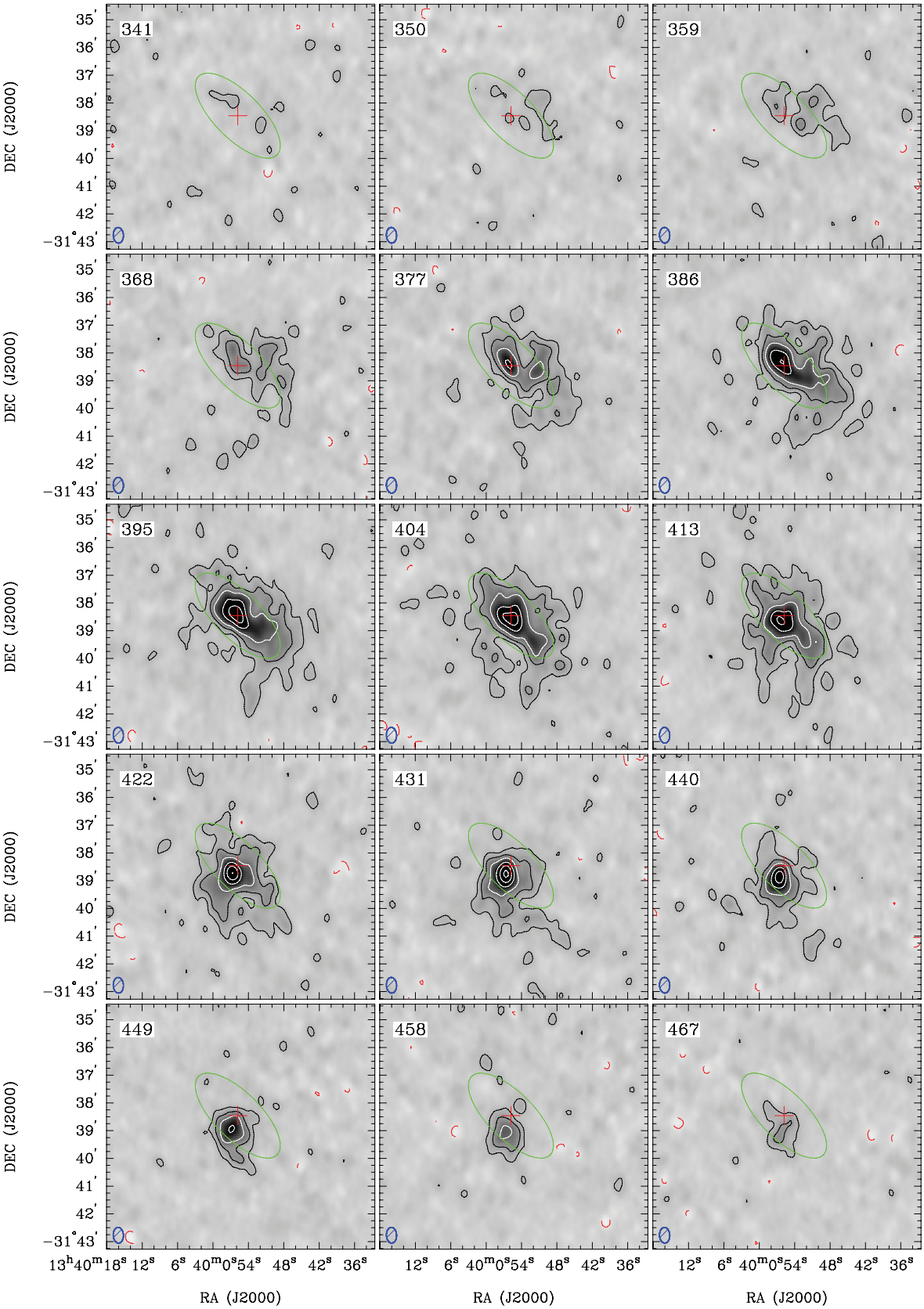

Figure 6. H I channel maps, in steps of 9 km s^{-1}, of the BCDG NGC 5253 as obtained from the ATCA, using 'robust' ($r = 0$) weighting and excluding baselines to CA06 (intermediate-resolution data cube). The contour levels are −2.5 (dashed red contours), 2.5 (∼2.6σ), 6, 12, 24, 36 and 48 mJy beam^{-1}. The galaxy centre is marked with a red cross, while the green ellipse corresponds in size to the optical appearance of the galaxy. The centre velocity of each channel is displayed at the top-left and the synthesized beam (33.9 × 22.1 arcsec^2) at the bottom-left corner of each panel.

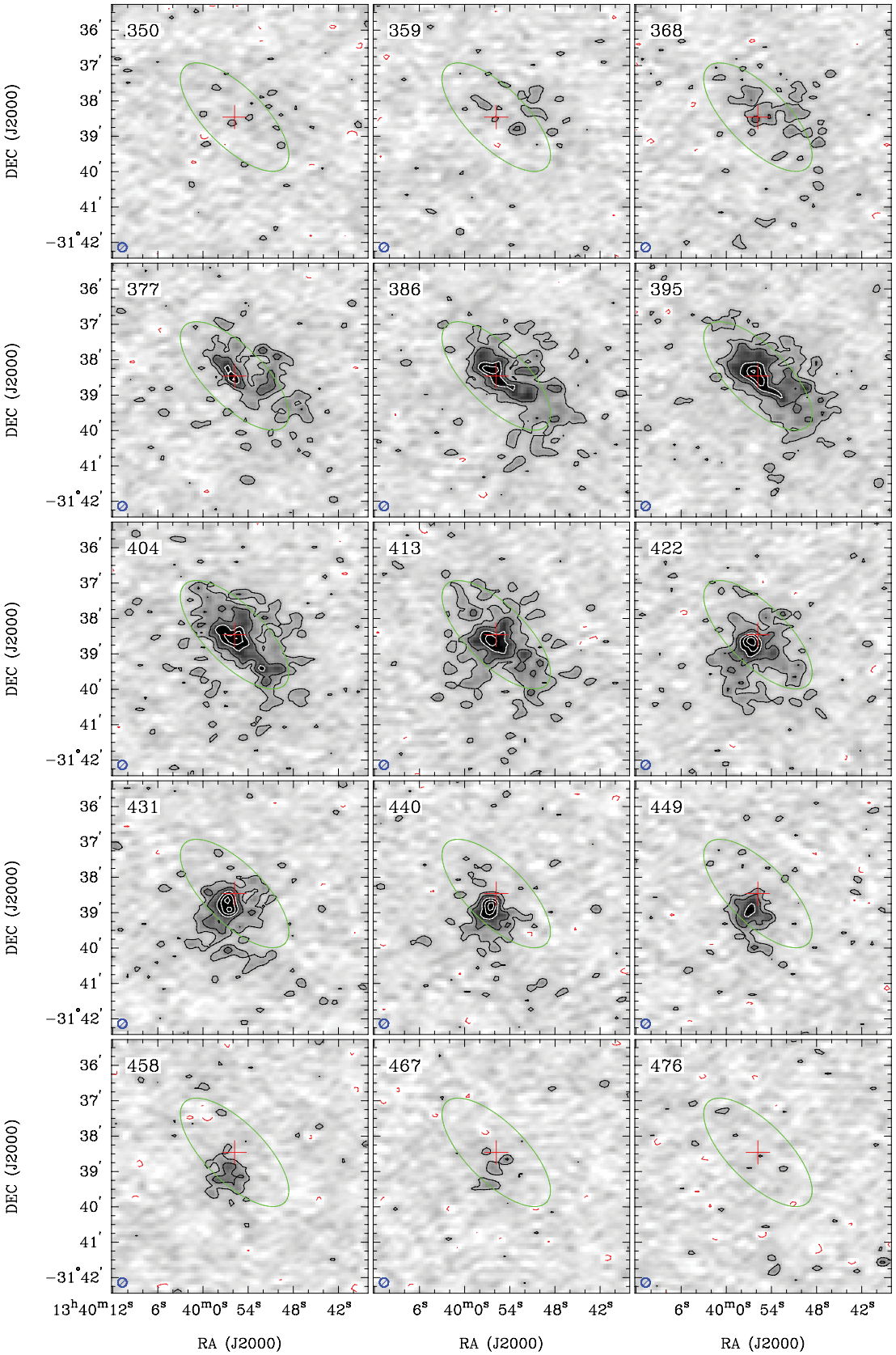

Figure 7. H I channel maps, in steps of 9 km s^{-1}, of the BCDG NGC 5253 as obtained from the ATCA, using 'robust' weighting ($r = 0$) and including baselines to CA06 (high-resolution data cube). The contour levels are -2.2 (dashed red contours), 2.2 ($\sim 2.5\sigma$), 5, 10, 15 and 20 mJy beam^{-1}. The galaxy centre is marked with a red cross, while the green ellipse corresponds in size to the optical appearance of the galaxy. The centre velocity of each channel is displayed at the top-left and the synthesized beam (15.0 × 15.0 arcsec^2) at the bottom-left corner of each panel.

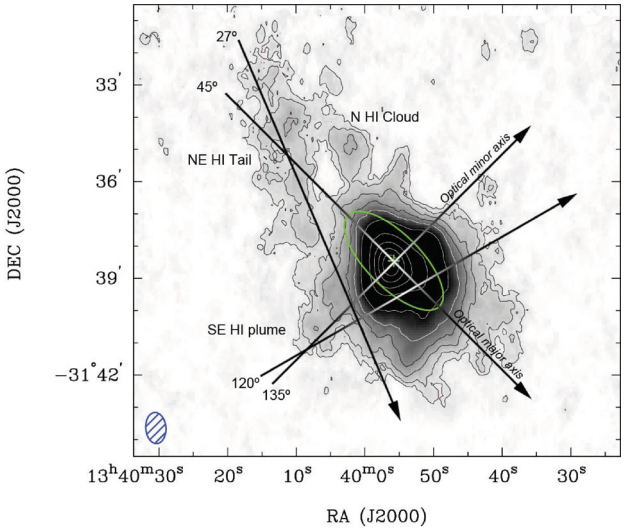

Figure 8. H I distribution map of NGC 5253 using our low-resolution data cube and showing the slit positions used to create the PV diagrams shown in Figs 9 and 10. The most prominent features have been labelled.

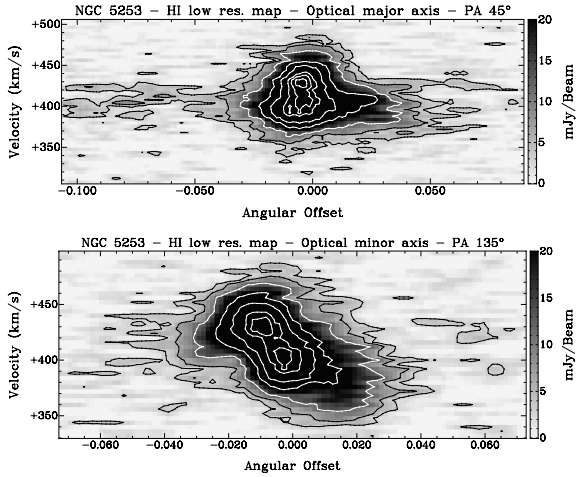

Figure 9. H I PV diagrams of NGC 5253 using our low-resolution data cube. The slits cross along the optical major axis (top panel, with PA = 45°, northeast is left) and along the optical minor axis (bottom panel, with PA = 135°, southeast is left). The units of the *x*-axis are radians, 0.1 rad are 5.°73 or 400 kpc at the distance of NGC 5253. The contour levels are: 3, 6, 12, 25, 40, 60, 70 and 80 mJy beam^{-1}. The slit positions are shown in Fig. 8.

origin. Hence, we propose that the very peculiar H I morphology and kinematics of NGC 5253 can be explained by an interaction scenario, in which the infall of an independent H I cloud along the minor axis of the galaxy is disturbing the existing neutral gas and triggering the powerful starburst. Both entities now seem to be in a process of merging, but the interaction probably started a long time ago, as we detect tidal gas at the northern regions of the galaxy and it seems that previous starbursts have occurred in the system. We also confirm the existence of a high-density H I bubble at the NW regions, which matches the Hα emission and seems to be a consequence of the combined actions of the winds of massive stars and supernova explosions. However, our H I data alone do not allow us to definitively confirm the proposed infall scenario, as some features (the long disturbed neutral gasat the NE and the compressed H I edge at the SW) may have also originated as the result of ram pressure stripping from moving through a dense IGM.

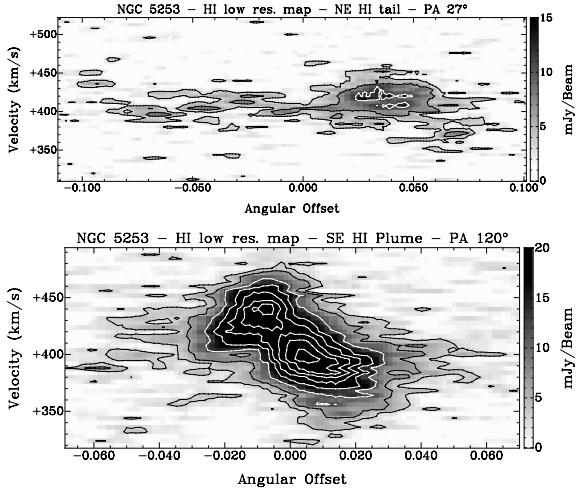

Figure 10. H I PV diagrams of NGC 5253 using our low-resolution data cube. The slits cross along the disturbed material at the NE of the galaxy (top panel, with PA = 27°, northeast is left) and along the 'SE H I plume' (bottom panel, with PA = 120°, southeast is left). The units of the *x*-axis are radians, 0.1 rad are 5.°73 or 400 kpc at the distance of NGC 5253. The contour levels are: 3, 6, 12, 24, 31, 38 and 44 mJy beam^{-1}. The slit positions are shown in Fig. 8.

4 20-CM RADIO-CONTINUUM EMISSION

Fig. 11 shows the contours of the 20-cm radio-continuum emission map of NGC 5253 and its comparison with the *GALEX FUV* band and Hα images. The radio-continuum emission within this BCDG is clearly resolved and has an extension of 0.6 × 1.0 arcmin^2. The 20-cm radio-continuum emission is located exactly at the centre of the galaxy, at the position where the powerful starburst (and almost all the *FUV* emission) is found, and shows an extension towards the SE. This faint feature may be related to an Hα arc that is located in this area.

We also detect faint emission at the NW of the galaxy, which is detached from the main 20-cm emission of NGC 5253. This object, which has a 1.4 GHz flux of 1.2 ± 0.2 mJy, is located over some faint Hα emission in the external region of the galaxy. However, it is probably a background radio source.

The total 20-cm radio-continuum flux we derive from NGC 5253, $S_{1.4\,\mathrm{GHz}}$ = 78 ± 3 mJy, is slightly lower than the value derived by Condon et al. (1996) in their 1.4 GHz VLA Atlas of bright *IRAS* galaxies, which was 83.8 mJy, although the synthesized beam size of their 20-cm radio-continuum map was larger (54 arcsec). Assuming that the galaxy lies at a distance of 4.0 Mpc and applying the expression given by Yun, Reddy & Condon (2001), we derive a 1.4 GHz luminosity of (1.47 ± 0.06) × 10^{20} W Hz^{-1} for NGC 5253.

5 DISCUSSION

5.1 The global star formation rate of NGC 5253 and nearby dwarf galaxies

The SFR of a galaxy can be estimated using different calibrations at many different wavelengths, from X-ray to radio. Here, we will consider the global SFR derived from (i) far-ultraviolet (*FUV*) images using the calibration provided by Salim et al. (2007), (ii) Hα images and the calibration given by Calzetti et al. (2007), (iii) far-infrared (*FIR*) data, in particular, the 60 μm flux with the calibration

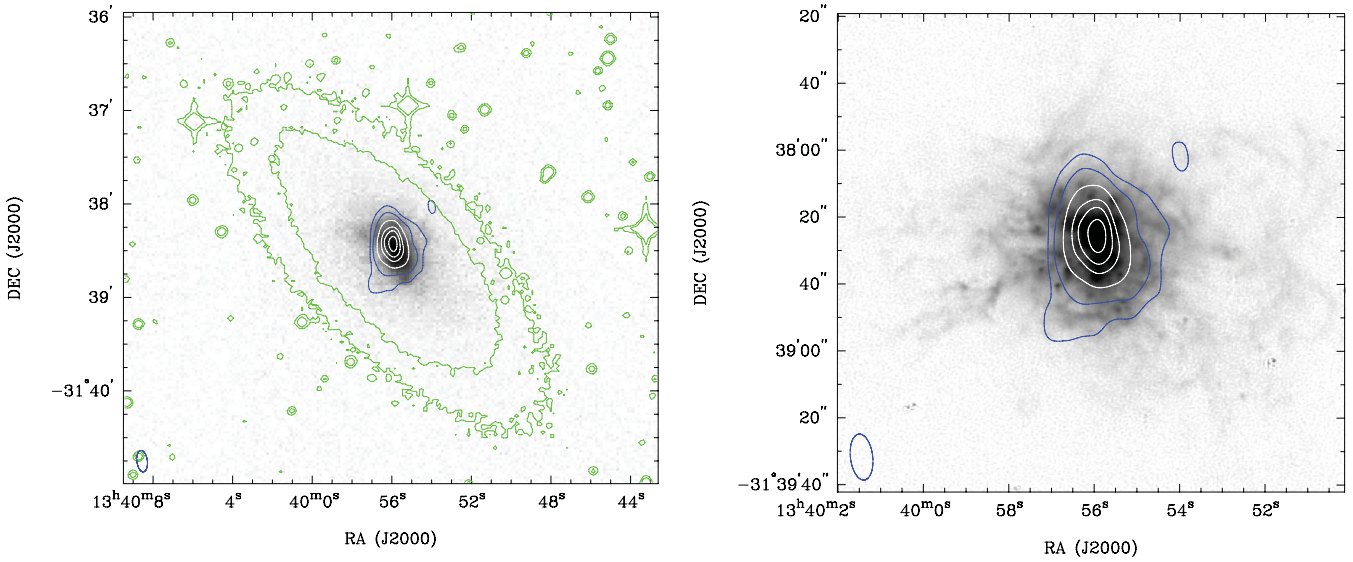

Figure 11. 20-cm radio-continuum contours of NGC 5253 overlapped on to a (left) *GALEX FUV*-band image and (right) an Hα image (Meurer et al. 2006), both images on logarithmic scale. The contours are −0.9, 0.9, 1.8, 4, 9, 14 and 22 mJy beam^{-1}. The left-hand panel shows the contours of the *R*-band image in green. The synthesized beam (13.8 × 6.7 arcsec^2) is displayed at the bottom-left corner in both panels.

Table 3. Luminosities and SFRs ($M_\odot$ yr^{-1}) of NGC 5253, ESO 444−G084, IC 4316 and NGC 5264.

Name HIPASS	NGC 5253 J1339−31A	IC 4316 J1340−28	ESO 444−G084 J1337−28	NGC 5264 J1341−29
$L_{\rm FUV}$ (10^{38} erg s^{-1} Å^{-1})	23.5 ± 1.5	1.54 ± 0.11	1.15 ± 0.14	2.18 ± 0.30
$L_{\rm H\alpha}$ (10^{38} erg s^{-1})	440 ± 20	∼1.90	4.10 ± 0.38	16.4 ± 2.9
$L_{60\,\mu\rm m}$ (10^{22} W Hz^{-1})	5.71 ± 0.01	...	...	0.0737 ± 0.0013
$L_{\rm FIR}$ (10^{41} erg s^{-1})	25.83 ± 0.09	...	...	0.475 ± 0.090
$L_{20\,\rm cm}$ (10^{19} W Hz^{-1})	14.7 ± 0.6	0.126 ± 0.039	<0.6	<0.7
$SFR_{\rm FUV}$ (S07)	0.190 ± 0.010	0.0125 ± 0.0009	0.0093 ± 0.0011	0.0177 ± 0.0025
$SFR_{\rm H\alpha}$ (C07)	0.233 ± 0.011	∼0.0010	0.0022 ± 0.0002	0.0087 ± 0.0015
$SFR_{60\,\mu\rm m}$	0.11	...	...	0.0014 ± 0.0003
$SFR_{\rm FIR}$	0.12	...	...	0.0021 ± 0.0004
$SFR_{\rm 20cm}$	0.176 ± 0.010	0.0015 ± 0.0005	<0.0071	<0.0086
Assumed *SFR*	0.20	0.0035	0.0070	0.0090

References: S07 = Salim et al. (2007) and C07 = Calzetti et al. (2007).

provided by Condon (1992) and the total *FIR* flux with the calibration given by Kennicutt (1998), and (iv) 20-cm radio-continuum data using the calibration provided by Condon, Cotton & Broderick (2002). A recent review of all these calibrations is provided by López-Sánchez (2010), who analysed the *SFRs* of a sample of strong starbursting systems (including NGC 5253) using multiwavelength data. For comparison purposes, we also computed the *SFRs* derived for the other dwarf galaxies of the M83 subgroup. Table 3 lists both the luminosities and the SFRs derived for these four galaxies using this multiwavelength analysis.

We note that the *FUV* and Hα luminosities quoted in Table 3 have been corrected for extinction in all galaxies using the A_B values indicated in Table 1 and following the prescriptions explained in López-Sánchez & Esteban (2008) and López-Sánchez (2010) for correcting the Hα and the *FUV* fluxes, respectively. The total Hα fluxes of the galaxies NGC 5253, ESO 444−G084 and NGC 5264 have been extracted from Meurer et al. (2006). To estimate the total Hα flux in IC 4316, we added the Hα flux of the six star-forming regions spectroscopically observed by Lee et al. (2007) within this galaxy. The value was corrected for reddening considering an average value for the $C_{\rm H\beta}$ coefficient these authors estimated for the star-forming regions, for which we derive $A_B \sim 0.63$ mag. However, the total Hα flux computed in this way underestimates the total Hα flux of IC 4316 because the spectroscopic data compiled by Lee et al. (2007) do not cover all the ionized gas detected in the galaxy. Considering the aperture sizes and the Hα map provided by these authors (see their fig. 2b) we estimate that the area recovered by the spectroscopic data is ∼20 per cent of all the region showing Hα emission. The values compiled in Table 3 consider this correction and, therefore, are only tentative estimations to the real Hα values.

For NGC 5253, the Hα-based and the *FUV*-based SFRs agree quite well. The *FIR*-based SFRs also are in agreement with those values; however, these SFR estimations have a larger uncertainty. Interestingly, the $\rm SFR_{20cm}$ value also agrees with them. Note that Hα emission traces the most recent star formation event (<10 Myr) but *FUV* and radio-continuum emission trace the star formation activity in the last ∼100 Myr. Hence, although the most recent star formation event happened ∼3.5 Myr ago (López-Sánchez et al. 2007) and the majority of the star clusters located in the centre of the

galaxy have ages younger than 10 Myr (Alonso-Herrero et al. 2004), the good agreement between all multiwavelength SFR indicators suggests that the elevated star formation activity has been present in NCG 5253 for several ∼100 Myr. This result agrees very well with the recent analysis presented by McQuinn et al. (2010a), b), who measured the duration of starbursts in 20 nearby, ongoing and *fossil* starbursts in dwarf galaxies, including NGC 5253. This analysis, based on the recent star formation histories derived from resolved stellar population data obtained with the *Hubble Space Telescope*, revealed that the starburst durations may range from 450 to 650 Myr (sometimes even ∼1.3 Gyr).

On the other hand, for the other galaxies the *FUV*-based SFR is always higher than the Hα-based SFR, with both quantities also higher than the SFR_{20cm}. This suggests that the recent star formation activity has decreased when compared with that experienced by the galaxies in the last ∼100 Myr. We note, however, that some recent analyses (i.e. Lee et al. 2009; Pflamm-Altenburg, Weidner & Kroupa 2009) indicate that the Hα luminosity underestimates the SFR relative to the *FUV* luminosity in dwarf galaxies with SFR ≤ 0.01 $M_{\odot}$ yr^{-1}. But the very low 20-cm radio-continuum flux estimated for these three galaxies strongly suggests that the star formation activity has not been strong recently.

5.2 Comparison of the neutral gas component of NGC 5253 with that found in other starbursts

We now compare the features of the neutral gas component found in NGC 5253 with the other starbursts described in the literature. Recent analyses of the neutral gas component of dwarf starburst galaxies include NGC 2366 (van Eymeren et al. 2009a), NGC 4861 (van Eymeren et al. 2009b), NGC 5408 and IC 4662 (van Eymeren et al. 2010). All these galaxies have the common characteristic of showing outflows of neutral gas that follows the ionized gas. Indeed, the minimum of the H I column density is usually found at the centre of these structures, as it happens in the NW region in NGC 5253 (see Fig. 3) where, as previously noticed by KS08, the H I shell spatially coincides with an Hα shell, and both structures seem to have similar expansion velocities (30–40 km s^{-1}). This effect seems to be a consequence of both (i) the consumption of the neutral gas to form new stars and (ii) the injection of kinetic energy into the ISM by the combined action of both winds from massive stars and supernova explosions, which pushes the ionized gas and creates a superbubble that may develop in a galactic wind. However, perhaps the large amount of neutral gas still found in these shells is responsible for stalling the expansion and prevents the formation of a galactic wind (KS08), and hence that is the reason why these are not found in dwarf galaxies. Therefore, the non-detections of galactic winds in dwarf starburst galaxies will contradict the theoretical models by Mac Low & Ferrara (1999) but will agree with the theoretical models developed by Silich & Tenorio-Tagle (1998). Following these models, the expansion velocity of the outflows will never get close to or beyond the escape velocity due to the presence of a dark matter halo (in our case, maybe the huge amount of neutral gas that is surrounding the main body of the galaxy is also playing an important role) that slows down the gas expelled by the galactic winds. In fact, the expansion velocities of the gas computed by van Eymeren et al. (2010) are 30–50 per cent the escape velocities.

A clear H I blowout is found in the dwarf irregular galaxy Holmberg I (Ho I), belonging to the M81 galaxy group (Ott et al. 2001; Walter et al. 2007). The H I maps presented by these authors reveal one single H I hole surrounded by a supergiant shell. This structure, which comprises ∼75 per cent of the total H I content of the galaxy, has a diameter of ∼1.7 kpc and covers about half of the optical extent of Ho I. The supergiant shell found in Ho I is explained by the strong stellar winds and supernova explosions within the starburst. It seems that part of the neutral gas has been lost to the IGM. But the agreement between the maps shown by Ott et al. (2001) in Ho I and those obtained here for NGC 5253 is rather small. Furthermore, the star formation activity is much higher in NGC 5253 than in Ho I. Both facts strongly suggest that NGC 5253 and Ho I are experiencing different star formation histories.

Outflows seem to be accompanied by both Hα and X-ray emission. For example, Skillman, Côté & Miller (2003) reported filaments of Hα emission in NGC 625 (another BCD and WR galaxy), which are related to blowouts as they trace the path of hot gas into the halo (Heiles 1993). Effectively, the soft X-ray map of NGC 625 (Bomans & Grant 1998) reveals hot gas emission ($T \sim 10^6$ K) which is associated with the ionized and neutral diffuse gas of the outflow. However, the 'H I SE plume' found in NGC 5253 is not associated with any Hα or X-ray emission. Actually, the X-ray emission extends preferentially to the SW of the nucleus in this galaxy (Summers et al. 2004, KS08), casting doubt on its origin as an outflow.

NGC 625 is another BCDG hosting a large number of WR stars. The ATCA H I moment maps of NGC 625 presented by Cannon et al. (2004) reveal that this galaxy also has perturbed neutral gas kinematics. These authors explain this following a blowout scenario which is the result of an spatially and temporally extended star formation event that the galaxy has experienced in the last 100 Myr. However, Cannon et al. (2004) reported that NGC 625 is indeed undergoing a solid-body rotation about its optical minor axis, as expected for an inclined rotating disc. Interestingly, their high- and low-resolution H I maps of NGC 625 agree well between them. However, the situation in NGC 5253 is different. The high-resolution H I maps are revealing the densest neutral gas in the galaxy, which is basically associated with the 'NW Hα + H I shell' and the 'SE H I plume'. However, the low-resolution H I map shows the diffuse neutral gas, which is mainly perturbed by external factors.

It is interesting to compare NGC 5253 with IC 10, which is the only known starburst within the Local Group. As NGC 5253, IC 10 is a low-metallicity [12 + log(O/H) = 8.26; Skillman, Kennicutt & Hodge 1989; Garnett 1990; Magrini & Gonçalves 2009], low-mass galaxy showing a high star formation activity (i.e. Hodge & Lee 1990; Leroy et al. 2006), high far-infrared emission (Melisse & Israel 1994) and non-thermal radio-continuum emission (Yang & Skillman 1993). The outer H I gas of IC 10 was discovered by Shostak & Skillman (1989) and studied further by Wilcots & Miller (1998). These authors characterized the neutral gas of IC 10 by a rotating disc embedded in an extended, clumpy and complex distribution of gas. Wilcots & Miller (1998) also noted that the feedback of the massive stars has shaped shells and bubbles in the neutral gas of IC 10. However, the complex distribution and kinematics of the extended neutral gas around IC 10 suggest that this galaxy is still accreting gas from the large, extended H I reservoir, and hence the starburst may have been probably triggered by this gas falling in.

Another interesting dwarf starbursting galaxy is NGC 1705. Meurer, Staveley-Smith & Killeen (1998) presented an analysis of the H I gas in this BCDG. They found not only an H I rotating disc structure, but also a neutral gas distribution that appears disturbed. They reported the detection of an 'H I spur', which has around 8 per cent of the total H I mass of the galaxy, extending at least 4.5 kpc to the halo. These authors explained this feature as a

consequence of an outflow. They estimated that $\sim 2 \times 10^7$ $M_\odot$ of neutral ISM gas has been expelled from the galaxy. This lscenario agrees with the outflow of ionized gas powered by central massive star clusters (Marlowe et al. 1995). Meurer et al. (1998) also considered the interaction origin of this feature, which may be an independent H I cloud that is in the process of merging with NGC 1705. They discarded this hypothesis because the optical appearance of the galaxy is not disturbed at all. As in NGC 1705, the optical distribution of NGC 5253 is also quite symmetric. However, in both cases the detection limit of the available optical images is $\mu_B \sim 24$–25 mag arcsec^{-1} (Lauberts & Valentijn 1989; Gil de Paz, Madore & Pevunova 2003), but the stellar features that may be associated with these H I spurs may be much fainter (e.g. López-Sánchez, Esteban & García-Rojas 2006; López-Sánchez & Esteban 2008) and hence very deep images ($\mu_B \sim 27$–28 mag arcsec^{-1}) are needed to detect these very faint features (e.g. Martínez-Delgado et al. 2009, 2010). Hence, we should not completely discard the hypothesis that the 'H I spur' detected by Meurer et al. (1998) in NGC 1705 actually has a tidal origin. A fundamental difference with NGC 5253 is that the 'H I spur' found in NGC 1705 is not dominating the H I dynamics of the galaxy, which follow a well-defined rotation pattern. But that is not the case for NGC 5253, where the effect of the 'SE H I plume' is completely masking the expected rotation of the galaxy, and it is strongly perturbing the dynamics of the BCDG.

van Eymeren et al. (2010) reported evidence of merging in the BCDG IC 4662, as its diffuse H I gas is somewhat distorted and it shows a tail of neutral gas. Indeed, spectroscopic observations (Hidalgo-Gámez, Masegosa & Olofsson 2001; López-Sánchez et al., in preparation) seem to reveal important physical and chemical differences in the ionized gas within this galaxy, which also indicate that this galaxy is actually formed by two entities in interaction. Hence, in IC 4662 we found not only both outflows of neutral and ionized gas surrounding the star-forming regions but also distortions in the neutral gas that seem to be originated by a galaxy merger.

Finally, we compare NGC 5253 with the BCDG NGC 1569, which also hosts a strong starburst (Waller 1991; González-Delgado et al. 1997; Buckalew & Kobulnicky 2006). This galaxy seems to have recently interacted with an independent H I cloud (Stil & Israel 1998, 2002; Mühle et al. 2005). It shows a rotation velocity of only 30 km s^{-1} (Heckman et al. 1995) but outflows with expansion velocities up to 100 km s^{-1} (Westmoquette, Smith & Gallagher 2008). The situation in this galaxy is quite similar to that found in NGC 5253: perturbed H I morphology and kinematics, high dispersion velocities of the central neutral gas, an almost inexistent rotation pattern, the probable detection of tidally ejected material, and outflows of both neutral (Stil & Israel 2002) and ionized (Westmoquette et al. 2007b) gas related to the violent star formation activity in the starburst. Hence, we conclude that the main peculiar characteristic of the neutral gas in NGC 5253 (i.e. the apparent rotation about its optical major axis following the 'SE H I plume') is naturally explained by the infall of an independent H I cloud and not by an outflow.

Summarizing, the comparison between NGC 5253 and a galaxy clearly hosting an outflow (Ho I) indicates that the nature of the H I gas has different origins. Furthermore, there is no Hα or X-ray emission associated with the 'SE H I plume'. However, the situation of NGC 5253 is similar to that observed in galaxies which seem to be in interaction with diffuse H I clouds (IC 10, IC 4662, NGC 625, NGC 1705) and it is almost identical to that seen in a galaxy which is certainly known to be experiencing an interaction event with an independent H I cloud (NGC 1569).

5.3 Environment of NGC 5253

NGC 5253 is located in the Centaurus A Group, which is one of the nearest galaxy groups within the Local Volume. It consists of two subgroupings (Karachentsev et al. 2002, 2007), one around Cen A (NGC 5128, which lies at 3.77 Mpc) and the other around M83 (NGC 5236, which is at a distance of 4.6 Mpc). This late-type spiral galaxy possesses an unusually large H I envelope (Koribalski 2005; Koribalski et al., in preparation), and it is surrounded by some dwarf irregular galaxies: ESO 444−G084, IC 4316, UGCA 365 (ESO 444−G078), NGC 5264 and NGC 5253. NGC 5253 lies at an angular distance of $\sim 1^\circ 54'$ and $\sim 12^\circ$ from M83 and Cen A, respectively.

However, its distance obtained using different methods gives different results (i.e. Saha et al. 1995; Gibson et al. 2000; Karachentsev et al. 2002, 2007; Thim et al. 2003; Sakai et al. 2004; Davidge 2007; Mould & Sakai 2008) ranging between 3.0 and 4.2 Mpc. Here we adopted 4.0 Mpc following Karachentsev et al. (2004). Hence, NGC 5253 is somewhat located at the periphery of the Cen A / M83 complex and between both subgroups. Karachentsev et al. (2007), however, located NGC 5253 in the Cen A subgroup, but this galaxy is not far away from ESO 444−G084, IC 4316 and NGC 5264, which lie at around 4.5 Mpc, all belonging to the M83 subgroup. The estimations of the distance to M83 range between 4.5 and 4.9 Mpc, here we consider it is at 4.6 Mpc (Karachentsev et al. 2002).

The morphology and kinematics of the H I gas within NGC 5253 are much more difficult to explain than that seen in the nearby galaxies IC 4316, ESO 444−G084 and NGC 5264 (see Koribalski et al. 2011 to see their H I maps). These three galaxies mainly show symmetric H I morphologies and a pattern of rotation, although some mild disturbances seem to be found in ESO 444−G084 and NGC 5264. In the latter case there is some evidence that the galaxy interacted with an independent object in the past. Current cosmological models indicate that purely isolated galaxies should be extremely rare. Indeed, we should expect to find distortions in the outer parts of the galaxies and, in some ways, it should be very difficult to find a 'pure' isolated system (Koribalski 2010). These disturbances reveal the processes that are building up the galaxies and are very evident in strong star-forming dwarf systems when deep data are available (e.g. López-Sánchez & Esteban 2008, 2009; López-Sánchez 2010). The peculiar morphology and kinematics of the H I gas reported here in NGC 5253 and the very intense starburst that this galaxy is experiencing strongly suggest a connection between both galaxy properties.

It is interesting to note that NGC 5253 is also close to the late-type spiral galaxy M83, which lies at a radial distance of only $\sim$600 kpc, their projected separation being $\sim$130 kpc. LVHIS data of this galaxy (Koribalski 2005; Koribalski et al., in preparation) are remarkable, as its H I distribution (which has a size of $\sim$100 kpc, i.e. at least five times larger than its optical Holmberg diameter) has streamers, irregular enhancements, and more interesting, an asymmetric tidal arm which points out to the direction of NGC 5253. This tidal structure indicates that M83 has accreted or strongly interacted with a dwarf galaxy in the past. Furthermore, Bresolin et al. (2009) reported an abrupt discontinuity in the radial oxygen abundance trend near the optical edge of the disc of M83, which they also associated with a past galaxy encounter. Could it be with NGC 5253? Previous authors (van den Bergh 1980; Caldwell & Phillips 1989) already suggested that the nuclear starburst observed in NGC 5253 was triggered as a result of an interaction with M83 around 1 Gyr ago. In this sense, the main disturbances in the H I distribution of NGC 5253 are precisely aligned in the direction to

the long H I tidal arm found in M83. Hence, our data may suggest that a diffuse H I filament between both galaxies exists, and part of it may be infalling NGC 5253. Indeed, the metallicity computed by Bresolin et al. (2009) in the external disc of M83 – 12 + log(O/H) ∼ 8.2 – is a good match to that estimated in NGC 5253. This diffuse gas stripped from the external H I disc of M83 may be the origin of the H I cloud that is infalling along the minor axis of NGC 5253. The fact that the real duration of the starburst in NGC 5253 may be longer than 450 Myr (McQuinn et al. 2010a,b) ties very well with either the ongoing infall that the galaxy may be experiencing now or the effects with an interaction with M83 that started well before the currently observed star formation burst.

5.4 Other peculiarities of NGC 5253

López-Sánchez (2010) analysed a sample of strong star-forming galaxies (WR galaxies) that included NGC 5253. He found that in contrast to that observed in starburst galaxies and in star-forming regions or *UV*-rich star clusters in spiral galaxies (Kennicutt et al. 2007; Koribalski & López-Sánchez 2009), NGC 5253 does not obey the Schmidt–Kennicutt (SK) scaling laws of star formation (Schmidt 1959, 1963; Kennicutt 1998).

López-Sánchez (2010) also compared the H I mass-to-light ratio (which is a distance-independent quantity) with the total stellar mass, $M_{\rm stars}$, for his galaxy sample (see his fig. 16). We reproduce this plot in our Fig. 12, his data points are the dark yellow squares. This figure also shows the position of the LVHIS galaxies analysed by Kirby et al. (2011) (red triangles) and the data points of the sample of nearby dwarf irregular galaxies studied by Lee et al. (2007) (stars). As noticed by López-Sánchez (2010), the position of NGC 5253 in this diagram clearly disagrees with the position of the other galaxies, as it shows an $M_{\rm H\,I}/L_B$ ratio that is an order of magnitude smaller than that expected from its stellar mass. We note that NGC 1569, which shares similar properties to those observed in NGC 5253 (including a probable interaction with an independent

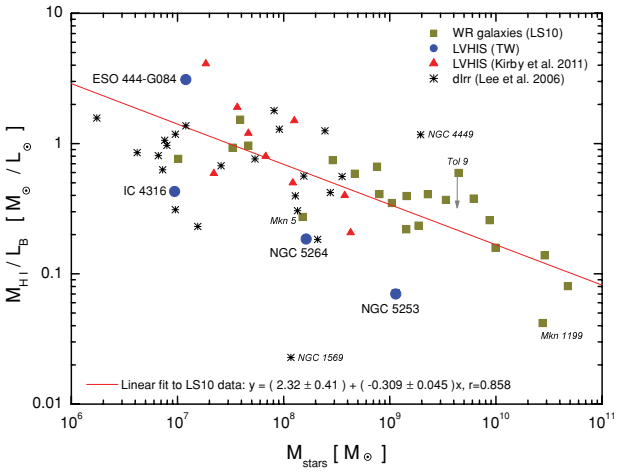

Figure 12. Comparison between the stellar mass, $M_{\rm stars}$, and the H I mass-to-light ratio for NGC 5253 and its nearby dwarf galaxies (blue circles). We compare with the sample of nearby dwarf irregular galaxies analysed by Lee et al. (2007), with the sub-sample of the LVHIS galaxies studied by Kirby et al. (2010) (red triangles), and with the sample of strong star-forming (WR) galaxies analysed by López-Sánchez (2010) (dark yellow squares), which included NGC 5253. The red solid line shows a linear fit to the López-Sánchez (2010) data.

H I cloud; see Section 5.2), also lies very far from the position of the other galaxies in the diagram plotted in Fig. 12.

López-Sánchez (2010) also compared the $M_{\rm gas}/M_{\rm stars}$ ratio and the oxygen abundance for his galaxy sample. His fig. 17 clearly shows that the $M_{\rm gas}/M_{\rm stars}$ ratio decreases with increasing metallicity, indicating that the importance of the stellar component to the total mass is larger in more massive galaxies. Indeed, galaxies show a clear correlation between the oxygen abundance and the total stellar mass (see the left-hand panel of fig. 14 in López-Sánchez 2010; Lara-López et al. 2010). Again, the position of NGC 5253 in this diagram does not agree with that observed for the rest of the galaxies, as it seems to have an approximately five times lower $M_{\rm H\,I}/L_B$ ratio than that expected for its metallicity. This may indicate that the oxygen abundance derived in the central, intense star-forming region is not reflecting the metallicity of the stellar component of the galaxy (i.e. the metallicity of stars born in previous star formation events), which may be higher than that derived from the analysis of the ionized gas. Assuming the derived $M_{\rm gas}/M_{\rm stars}$ ratio for NGC 5253, we should expect that this galaxy has a metallicity up to 0.3–0.4 dex higher than that computed in the central starburst [12 + log(O/H) = 8.18 ± 0.03; López-Sánchez et al. 2007]. Hence, the infall of low-metallicity neutral gas that we suggest here may have lowered the gas-phase abundance of this galaxy. Interestingly, López-Sánchez et al. (2007) found that the youngest starbursts – regions A and B, with 12 + log(O/H)= 8.18 ± 0.03 – have a metallicity which is ∼0.1 dex lower than that reported in slightly older areas – regions C and D, with 12 + log(O/H)= 8.30 ± 0.05.

Köppen & Hensler (2005) created chemical evolution models that consider massive and rapid accretion of metal-poor gas into a galaxy. They found that the oxygen abundance is decreased during the infall due to the dilution of the galactic gas, and that gas masses of 10^6 $M_\odot$ would be sufficient to cause a large influence on dwarf galaxies. They concluded that such a collision could leave observable marks in the chemical properties of the galaxies, different from what a closed-box evolution predicts. Indeed, NGC 5253 does not follow a close-box model (see fig. 21 in López-Sánchez 2010), as it happens in the majority of the WR galaxies analysed by this author. Actually, all the predictions indicated by Köppen & Hensler (2005) are satisfied in the case of NGC 5253, who also predicted that the galaxy may be very bright if the infall triggers enhanced star formation. Hence, the hypothesis of the infall of an H I cloud in NGC 5253 will naturally explain its relatively high baryonic mass for its oxygen abundance (see the left-hand panel of fig. 14 in López-Sánchez 2010), its very low $M_{\rm H\,I}/L_B$ ratio (and its position in Fig. 12) and its deviation of the SK scaling laws of star formation. Furthermore, our observational hypothesis agrees very well with the theoretical models recently presented by McKernan, Maller & Ford 2010, who predicted that the accretion of warm halo clouds will produce a nuclear starburst of low-metallicity stars in the centre of galaxies.

6 CONCLUSIONS

We have presented deep H I line and 20-cm radio-continuum data of the intriguing BCDG NGC 5253. The data were obtained not only using the ATCA as part of the LVHIS survey, but also from our multiwavelength analysis of BCDGs. Hence, we completed our study using multiwavelength data extracted from the literature, which includes X-ray, *FUV*, optical *B* and *R* band, Hα, *NIR H* band, and *FIR* data.

Our deep low-resolution H I maps show, for the first time, the very disturbed H I morphology that NGC 5253 possesses in its external

areas, which includes tails, plumes and detached H I clouds. Our data recover almost 96 per cent of the single-dish H I flux, indicating that very few diffuse emission has been filtered out in our interferometric observations. We derive a total H I mass of 1.59×10^8 $M_\odot$ in NGC 5253; around 5 per cent of this mass ($\sim 8 \times 10^6$ $M_\odot$) is located in the diffuse, almost detached gas found at the northern area of the galaxy. Adding the stellar mass to the neutral gas mass, we estimate that the baryonic mass of NGC 5253 is 13.5×10^8 $M_\odot$.

The high-resolution H I maps trace an Hα shell at the NW of the galaxy, which has a mass of $\sim 5.4 \times 10^6$ $M_\odot$, and it is related to an expanding bubble in the ISM that seems to be a consequence of the combined actions of the winds of massive stars and supernova explosions. However, this expanding bubble will almost certainly not end in a galactic wind. Our high-resolution H I maps also confirm the discovery of a 'SE H I plume' made by KS08, which is now clearly detected. This feature is not associated with any Hα or X-ray emission and hence it is most likely not related to an outflow. Indeed, the kinematics of the neutral gas in NGC 5253 derived from the low- and medium-resolution H I maps are highly perturbed and do not follow a rotation pattern. We argued that this feature actually is an independent H I cloud which is interacting with the main body of the galaxy. However, the H I data may also suggest that some of the features observed in NGC 5253 have originated as the result of ram pressure stripping from moving through a dense IGM.

Our 20-cm radio-continuum maps show that the emission of NGC 5253 is resolved and associated with the intense star-forming region located at the centre of the galaxy. We estimate the SFR using a multiwavelength approach, and compare the results with other galaxy properties. NGC 5253 does not satisfy the SK law of star formation, has a very low H I mass-to-light ratio when comparing with its stellar mass and seems to be slightly metal-deficient in comparison with starburst galaxies of a similar baryonic mass. The relatively high stellar mass also indicates that the BCDG has experienced a relatively long star formation history.

We have compared the properties observed in NGC 5253 with those seen in three nearby galaxy members of the M83 subgroup (IC 4316, ESO 444−G084 and NGC 5264, for which we have also derived their properties using the data provided by the LVHIS survey) and with the properties found in other starbursting dwarf galaxies.

Taking into account all available observational data and the comparison with similar starbursting galaxies, we conclude that NGC 5253 is very probably experiencing the infall of a diffuse, low-metallicity H I cloud along the minor axis of the galaxy. The infall of this independent H I cloud is comprising the ISM and triggering the powerful central starburst. Both entities seem to be now in a process of merging, but the interaction probably started some time ago, as we detect tidal gas at the northern regions of the galaxy and it seems that previous starbursts have occurred in the system. Perhaps the origin of this low-metallicity H I cloud is related to the very asymmetric tidal H I arm detected in M83, which may indicate that both galaxies have experienced a strong interaction in the past.

This study reinforces the conclusions reached by López-Sánchez (2006, 2010), which suggests that interactions with or between dwarf galaxies or H I clouds trigger the star formation activity in many dwarf and normal starburst galaxies.

Following the proposed infall scenario, perhaps the combined actions of the accretion of low-metallicity gas and the outflow found at the NW of the galaxy (which is now moving the metal-rich material into the surrounding IGM) have lowered the total oxygen abundance of NGC 5253, as its mass-to-light and mass-to-mass ratios seem to match better with an object with metallicities up to 0.3–0.4 dex higher than those computed in the youngest starburst. Hence, we conclude that a detailed and comprehensive multiwavelength analysis, such as this presented here, is a powerful tool to elucidate the complex relationships between star formation activity and the structure of the inner and external ISM, as well as to constrain the evolution and fate of the gas in star-forming galaxies.

ACKNOWLEDGMENTS

We thank the referee, Evan D. Skillman, for his detailed review of the article, which helped in improving the quality of this paper. This work is based on observations made with the ATCA, which is funded by the Commonwealth of Australia for operation as a National Facility managed by CSIRO. This research has made extensive use of the NASA/IPAC Extragalactic Data base (NED) which is operated by the Jet Propulsion Laboratory, Caltech, under contract with the National Aeronautics and Space Administration. The Digitised Sky Survey was produced by the Space Telescope Science Institute (STScI) and is based on photographic data from the UK Schmidt Telescope, the Royal Observatory Edinburgh, the UK Science and Engineering Research Council, and the Anglo-Australian Observatory. The *GALEX* is a NASA Small Explorer, launched in 2003 April. We gratefully acknowledge NASA's support for construction, operation and science analysis for the *GALEX* mission. This research has made extensive use of the SAO/NASA Astrophysics Data System Bibliographic Services (ADS). This publication makes use of data products from the Two Micron All Sky Survey, which is a joint project of the University of Massachusetts and the Infrared Processing and Analysis Center/California Institute of Technology, funded by the National Aeronautics and Space Administration and the National Science Foundation.

REFERENCES

Alonso-Herrero A., Takagi T., Baker A. J., Rieke G. H., Rieke M. J., Imanishi M., Scoville N. Z., 2004, ApJ, 612, 222
Asplund M., Grevesse N., Sauval A. J., 2005, in Bash F. N., Barnes T. G., eds, ASP Conf. Ser. Vol. 335, Cosmic Abundances as Records of Stellar Evolution and Nucleosynthesis. Astron. Soc. Pac., San Francisco, p. 25
Barnes D. G. et al., 2001, MNRAS, 322, 486
Beck S. C., Turner J. L., Ho P. T. P., Lacy J. H., Kelly D. M., 1996, ApJ, 457, 610
Bessel M. S., Castelli F., Plez B., 1998, A&A, 333, 231
Bomans D. J., Grant M.-B., 1998, Astron. Nachr., 319, 26
Bresolin F., Ryan-Weber E., Kennicutt R. C., Goddard Q., 2009, ApJ, 695, 580
Buckalew B. A., Kobulnicky H. A., 2006, AJ, 132, 1061
Caldwell N., Phillips M. M., 1989, ApJ, 338, 789
Calzetti D., Meurer G. R., Bohlin R. C., Garnett D. F., Kinney A. L., Leitherer C., Storchi-Bergmann T., 1997, AJ, 114, 1834
Calzetti D., Harris J., Gallagher J. S., III, Smith D. A., Conselice C. J., Homeier N., Kewley L., 2004, AJ, 127, 1405
Calzetti D. et al., 2007, ApJ, 666, 870
Campbell A., Terlevich R., Melnick J., 1986, MNRAS, 223, 811
Cannon J. M., McClure-Griffiths N. M., Skillman E. D., Côté S., 2004, ApJ, 607, 274
Colina L., Bohlin R. C., Castelli F., 1996, AJ, 112, 307
Condon J. J., 1992, ARA&A, 30, 575
Condon J. J., Helou G., Sanders D. B., Soifer B. T., 1996, ApJS, 103, 81
Condon J. J., Cotton W. D., Broderick J. J., 2002, AJ, 124, 675
Cresci G., Vanzi L., Sauvage M., 2005, A&A, 433, 447
Davidge T. J., 2007, AJ, 134, 1799
de Vaucouleurs G., de Vaucouleurs A., Corwin H. G., Jr, Buta R. J., Paturel G., Fouqué P., 1991, Third Reference Catalogue of Bright Galaxies. Springer Verlag, New York (RC3)

Garnett D. R., 1990, ApJ, 363, 142
Gibson B. K. et al., 2000, ApJ, 529, 723
Gil de Paz A., Madore B. F., Pevunova O., 2003, ApJS, 147, 29
González-Delgado R. M., Leitherer C., Heckman T., Cerviño M., 1997, ApJ, 483, 705
Gonzalez-Riestra R., Rego M., Zamorano J., 1987, A&A, 186, 64
Harris J., Calzetti D., Gallagher J. S., Smith D. A., Conselice C. J., 2004, ApJ, 603, 503
Heckman T. M., Dahlem M., Lehnert M. D., Fabbiano G., Gilmore D., Waller W. H., 1995, ApJ, 448, 98
Heiles C., 1993, Rev. Modern Astron., 6, 19
Hidalgo-Gámez A. M., Masegosa J., Olofsson K., 2001, A&A, 369, 797
Hodge D. A., Lee M. G., 1990, PASP, 102, 26 (HL90)
Jones D. H., Saunders W., Read M., Colless M., 2005, PASA, 22, 277
Kaldare R., Colless M., Raychaudhury S., Peterson B. A., 2003, MNRAS, 339, 652
Karachentsev I. D. et al., 2002, A&A, 385, 21
Karachentsev I. D., Karachentseva V. E., Huchtmeier W., Makarov D. I., 2004, AJ, 127, 2031
Karachentsev I. D. et al., 2007, AJ, 133, 504
Kennicutt R. C., Jr, 1998, ApJ, 498, 541
Kennicutt R. C., Jr et al., 2007, ApJ, 671, 333
Kirby E. M., Jerjen H., Ryder S. D., Driver S. P., 2008, AJ, 136, 1866
Kirby E. M., Koribalski B. S., Jerjen H., López-Sánchez Á. R., 2011, MNRAS, submitted
Kobulnicky H. A., Skillman E. D., 1995, ApJ, 454, L121
Kobulnicky H. A., Skillman E. D., Roy J.-R., Walsh J. R., Rosa M. R., 1997, ApJ, 277, 679
Kobulnicky H.A, Skillman E. D., 2008, AJ, 135, 527 (KS08)
Köppen J., Hensler G., 2005, A&A, 434, 531
Koribalski B. S., 2005, PASP, 22, 331
Koribalski B. S., 2008, in Koribalski B. S., Jerjen H., eds, Galaxies in the Local Volume. Springer, the Netherlands, p. 41
Koribalski B. S., 2010, Proc. Conf. Galaxies in Isolation: Exploring Nature versus Nurture hold at Granada (Spain) on 12–15 May 2009, in press
Koribalski B. S., López-Sánchez Á. R., 2009, MNRAS, 400, 1749
Koribalski B. S. et al., 2004, AJ, 128, 16
Lara-López M. A. et al., 2010, A&A, 521, 53
Lauberts A., Valentijn E. A., 1989, The Surface Photometry Catalogue of the ESO-Uppsala Galaxies. ESO, Garching bei München
Lee H., Grebel E. K., Hodge P. W., 2003, A&A, 40, 141
Lee H., Zucker D. B., Grebel E. K., 2007, MNRAS, 376, 820
Lee J. C. et al., 2009, ApJ, 706, 599
Leroy A., Bolatto A., Walter F., Blitz L., 2006, ApJ, 643, 825
López-Sánchez Á. R., 2006, Massive Star Formation in Dwarf Wolf-Rayet galaxies. PhD thesis, La Laguna University, Tenerife, Spain
López-Sánchez Á. R., 2010, A&A, 521, 63
López-Sánchez Á. R., Esteban C., 2008, A&A, 491, 131
López-Sánchez Á. R., Esteban C., 2009, A&A, 508, 615
López-Sánchez Á. R., Esteban C., 2010a, A&A, 516, 104
López-Sánchez Á. R., Esteban C., 2010b, A&A, 517, 85
López-Sánchez Á. R., Esteban C., García-Rojas J., 2006, A&A, 449, 997
López-Sánchez Á. R., Esteban C., García-Rojas J., Peimbert M., Rodríguez M., 2007, ApJ, 656, 168
López-Sánchez Á. R., Koribalski B. S., Esteban C., García-Rojas J., 2008, in Koribalski B. S., Jerjen H., eds, Proc. Galaxies in the Local Volume, Astrophysics and Space Science Proceedings, Springer, p. 53
López-Sánchez Á. R., Koribalski B. S., Esteban C., Popping A., van Eymeren J., Hibbard J., 2009a, Proc. Workshop Star forming galaxies: Following Ariadne's Thread in the Cosmic Labyrinth hold at Crete (Greece) on 29 September to 03 October 2008, in press
López-Sánchez Á. R., Koribalski B. S., Esteban C., Popping A., van Eymeren J., Hibbard J., 2010, ASP Conf. Proc. Vol. 421, Galaxies in Isolation: Exploring Nature versus Nurture. Astron. Soc. Pac., San Francisco, p. 65
Mac Low M-M., Ferrara A., 1999, ApJ, 513, 142
McKernan B., Maller A., Ford K. E. S., 2010, ApJ, 718, L83
McQuinn K. B. W. et al., 2010a, ApJ, 721, 297
McQuinn K. B. W. et al., 2010b, ApJ, 724, 49
Magrini L., Gonçalves D. R., 2009, MNRAS, 398, 280
Marlowe A. T., Heckman T. M., Wyse R. F. G., Schommer R., 1995, ApJ, 438, 563
Martin C. L., 1998, ApJ, 506, 222
Martin C. L., Kobulnicky H. A., Heckman T. M., 2002, ApJ, 574, 663
Martín-Hernández N. L., Schaerer D., Savage M., 2005, A&A, 429, 449
Martínez-Delgado D., Pohlen M., Gabany R. J., Majewski S. R., Peñarrubia J., Palma C., 2009, ApJ, 692, 955
Martínez-Delgado D. et al., 2010, AJ, 140, 962
Mayya Y. D., Bressan A., Carrasco L., Hernández-Martínez L., 2006, ApJ, 649, 172
Meier D. S., Turner J. L., Beck S. C., 2002, AJ, 124, 877
Melisse J. P. M., Israel F. P., 1994, A&AS, 103, 391
Meurer G. R., Staveley-Smith L., Killeen N. E. B., 1998, MNRAS, 300, 705
Meurer G. R. et al., 2006, ApJS, 165, 307
Minchin et al., 2003, MNRAS, 346, 787
Monreal Ibero A., Vílchez J. M., Walsh J. R., Muñoz-Tuñón C., 2010, A&A, 517, 27
Moorwood A. F. M., Glass I. S., 1982, A&A, 115, 84
Mould J., Sakai S., 2008, ApJ, 686, 75
Mühle S., Klein U., Wilcots E. M., Hüttemeister S., 2005, AJ, 130, 524
Ott J., Walter F., Brinks E., Van Dyk S. D., Dirsch B., Klein U., 2001, AJ, 122, 3070
Paturel G., Theureau G., Bottinelli L., Gouguenheim L., Coudreau-Durand N., Hallet N., Petit C., 2003, A&A, 412, 57
Pflamm-Altenburg J., Weidner C., Kroupa P., 2009, MNRAS, 395, 394
Rieke G. H., Lebofsky M. J., Walker C. E., 1988, ApJ, 325, 679
Saha A., Sandage A., Labhardt L., Schwengeler H., Tammann G. A., Panagia N., Macchetto F. D., 1995, ApJ, 438, 8
Sakai S., Ferrarese L., Kennicutt R. C., Jr, Saha A., 2004, ApJ, 608, 42
Salim S. et al., 2007, ApJS, 173, 267
Sault R. J., Teuben P. J., Wright M. C. H., 1995, in Shaw R., Payne H. E., Hayes J. J. E., eds, ASP Conf. Ser. Vol. 77, Astronomical Data Analysis Software and Systems IV. Astron. Soc. Pac., San Francisco, p. 433
Schaerer D., Contini T., Kunth D., Meynet G., 1997, ApJ, 481, L75
Schlegel D. J., Finkbeiner D. P., Davis M., 1998, ApJ, 500, 525
Schmidt M., 1959, ApJ, 129, 243
Schmidt M., 1963, ApJ, 137, 758
Shostak G. S., Skillman E. D., 1989, A&A, 214, 33
Silich S. A., Tenorio-Tagle G., 1998, MNRAS, 299, 249
Skillman E. D., Kennicutt R. C., Hodge P. W., 1989, ApJ, 347, 875
Skillman E. D., Côté S., Miller B. W., 2003, AJ, 125, 593
Skrutskie M. F. et al., 2006, AJ, 131, 1163
Stil J. M., Israel F. P., 1998, A&A, 337, 64
Stil J. M., Israel F. P., 2002, A&A, 392, 473
Strickland D. K., Stevens I. R., 1999, MNRAS, 306, 43
Summers L. K., Stevens I. R., Strickland D. K., Heckman T. M., 2004, MNRAS, 351, 1
Thim F., Tammann G. A., Saha A., Dolphin A., Sandage A., Tolstoy E., Labhardt L., 2003, ApJ, 590, 256
Turner J. L., Beck S. C., 2004, ApJ, 602, 85
Turner J. L., Beck S. C., Hurt R. L., 1997, ApJ, 474, L11
Turner J. L., Ho P. T. P., Beck S. C., 1998, AJ, 116, 1212
van den Bergh S., 1980, PASP, 92, 122
van Eymeren J., Marcelin M., Koribalski B. S., Dettmar R.-J., Bomans D. J., Gach J.-L., Balard P., 2009a, A&A, 493, 511
van Eymeren J., Marcelin M., Koribalski B. S., Dettmar R.-J., Bomans D. J., Gach J.-L., Balard P., 2009b, A&A, 505, 105
van Eymeren J., Koribalski B. S., López-Sánchez Á. R., Dettmar R.-J., Bomans D. J., 2010, MNRAS, 407, 113
Vanzi L., Sauvage M., 2004, A&A, 415, 509
Waller W. H., 1991, ApJ, 370, 144
Walsh J. R., Roy J.-R., 1989, MNRAS, 239, 297

Walter F. et al., 2007, ApJ, 661, 102
Warren B. E., Jerjen H., Koribalski B. S., 2004, AJ, 128, 1152
Westmoquette M. S., Smith L. J., Gallagher J. S., Exter K. M., 2007, MNRAS, 381, 913
Westmoquette M. S., Smith L. J., Gallagher J. S., 2008, MNRAS, 383, 864
Wilcots E. M., Miller B. W., 1998, AJ, 116, 2363
Yang H., Skillman E. D., 1993, AJ, 106, 1448
Yun M. S., Reddy N. A., Condon J. J., 2001, ApJ, 554, 803

This paper has been typeset from a TEX/LATEX file prepared by the author.